Title: Resting natural killer cells promote the progress of colon cancer liver metastasis by elevating tumor-derived sSCF

Author(s) and affiliation(s):
Chenchen Mao[1,2,#], Yanyu Chen[2,3,#], Dong Xing[2,#], Teming Zhang[2,#], Dianfeng Mei[2], Zheng Han[2], Wangkai Xie[2], Cong Long[2], Yangxuan Lin[4] , Jiaye Yu[2], Dan Xiang[2,*], Mingdong Lu[1,*], Xian Shen[5,*], and Xiangyang Xue[1,2,*]

[1]Department of General Surgery, The Second Affiliated Hospital and Yuying Children's Hospital of Wenzhou Medical University, Wenzhou, China.
[2]Department of Microbiology and Immunology, Institute of Molecular Virology and Immunology, School of Basic Medical Sciences, Wenzhou Medical University, Wenzhou, China.
[3]Department of Pediatric Thoracic Surgery, The Second Affiliated Hospital and Yuying Children's Hospital of Wenzhou Medical University, Wenzhou, China.
[4]Department of Thoracic Surgery, The First Affiliated Hospital of Wenzhou Medical University, Wenzhou, China.
[5]Department of General Surgery, The First Affiliated Hospital of Wenzhou Medical University, Wenzhou, China.

[#]These authors contributed equally: Chenchen Mao, Yanyu Chen, Dong Xing and Teming Zhang.

Running title: Resting NK cells and colon cancer liver metastasis

*Correspondence should be addressed to,
Xian Shen, Ph.D
Tel: +13968888872
Chashan Higher Education Park, Ouhai District, Wenzhou City, Zhejiang Province
shenxian@wmu.edu.cn

Xiangyang Xue, Ph.D.
Tel: +15058788169
Chashan Higher Education Park, Ouhai District, Wenzhou City, Zhejiang Province
wzxxy@wmu.edu.cn

Mingdong Lu
Tel: +18757791206
No.1111 East Section of Wenzhou Avenue, Longwan District, Wenzhou City, Zhejiang Province
lumd@wmu.edu.cn

Dan Xiang, Ph.D.
Tel: +13587689767

Chashan Higher Education Park, Ouhai District, Wenzhou City, Zhejiang Province
xiangdan@wmu.edu.cn

Conflict of interest disclosure:
The authors declare no competing interests.

Abstract

Purpose: The abundance and biological contribution of Natural killer (NK) cells in cancer are controversial. Here, we aim to uncover clinical relevance and cellular roles of NK cells in colon cancer liver metastasis (CCLM)

Methods: We integrated single-cell RNA sequencing, spatial transcriptomics, and bulk RNA-sequencing datasets to investigate NK cells' biological properties and functions in the microenvironment of primary and liver metastatic tumors. Results were validated through an in vitro co-culture experiment based on bioinformatics analysis.

Results: We used single-cell RNA sequencing and spatial transcriptomics to map the immune cellular landscape of colon cancer and well-matched liver metastatic cancer. We discovered that GZMK+ resting NK cells increased significantly in tumor tissues and were enriched in the tumor regions of both diseases. After combining bulk RNA and clinical data, we observed that these NK cell subsets contributed to a worse prognosis. Meanwhile, KIR2DL4+ activated NK cells exhibited the opposite position and relevance. Pseudotime cell trajectory analysis revealed the evolution of activated to resting NK cells. In vitro experiments further confirmed that tumor-cell-co-cultured NK cells exhibited a resting status, as evidenced by decreased KIR2DL4 expression. Functional experiments finally revealed that NK cells exhibited tumor-activating characteristics by promoting the dissociation and release of SCF on the tumor cells membrane depending on cell-to-cell interaction, as the supernatant of the co-culture system enhanced tumor progression.

Conclusion: Together, our findings revealed a population of protumorigenic NK cells that may be exploited for novel therapeutic strategies to improve therapeutic outcomes for patients with CCLM.

Keywords: Single cell RNA-sequencing, Spatial transcriptomics, Colon cancer liver metastasis, Natural killer cells

Introduction

Colon cancer is one of the most common malignancies, with more than 1 million new cases and 500 thousand deaths reported globally in 2020***(Sung et al., 2021)***. Approximately 19–26% of patients with colon cancer present with synchronous metastatic diseases at the first diagnosis***(Siegel et al., 2020)***, among which 14.5–17.5% develop liver metastasis***(Siegel, Miller, 2020, Wang et al., 2023)***. Although progress in the treatment of metastatic disease, including improved diagnosis and treatment strategies for liver metastases***(Chua et al., 2011, Zampino et al., 2016, Ruers et al., 2017)***, increased cancer-directed surgery***(Wancata et al., 2016)***, and the development of targeted therapies***(Piawah et al., 2019)***, has greatly improved the survival of these patients in recent decades, the 2-year relative survival rate for patients diagnosed with distant-stage disease was 36%***(Siegel, Miller, 2020)***, significantly lower than those without metastasis. Thus, colon cancer-derived liver metastasis (CCLM) is a clinical challenge that requires urgent development of novel treatment methods.

The tumor microenvironment (TME) is a dynamic environment that governs tumor behavior and is required for tumor cell survival, growth, proliferation, and metastasis***(Yao et al., 2023)***. Unlike previous understanding, it has recently been proposed that certain immune cells present in the TME (such as myeloid-derived suppressor cells***(Liu et al., 2023)***, macrophages***(Ngambenjawong et al., 2017)***, neutrophils***(Li et al., 2019)***, and $CD8^+$ T cells***(Tiberti et al., 2022)***) favor tumor progression. Thus, the contradictory findings of the pro- and anti-tumor effects of tumor-infiltrating immune cells require a better understanding of the immune features and profile heterogeneity of CCLM for the future development of immune-modulatory strategies to stratify and target immune cells.

Natural killer (NK) cells, an important component of tumor-infiltrating immune cells, are cytotoxic lymphocytes that play a key role in recognizing and eliminating malignant cells and are therefore considered the early responders against tumors***(Maskalenko et al., 2022)***. Among various immune cells, tumor-infiltrating NK cells are associated with prognosis in various cancers, such as colorectal cancer (CRC)***(Zhong et al., 2022)***, lung cancer***(Villegas et al., 2002)***, and gastric cancer***(Ishigami et al., 2000)***. Recently, based on their anti-tumor potential, NK cells were exploited for treating malignancies and have proven to be highly promising for the treatment of certain hematologic malignancies***(Lamb et al., 2021, Liu et al., 2020)*** but have limited efficacy for treating solid tumors***(Zhang et al., 2024, Hu et al., 2019, Oh et al., 2019)***. Additionally, intratumor NK cells differ phenotypically or functionally from peripheral NK cells in several malignancies***(Bruno et al., 2013, Carrega et al., 2008)***; a specific subset of tumor-infiltrating NK cells ($CD11b^-$ and $CD27^-$) was associated with tumor progression in lung and hepatocellular cancers***(Zhang et al., 2017, Jin et al., 2013)***. Notably, the tumor-promoting transformation of NK cells may be educated by cancer cells***(Chan et al., 2020, Huergo-Zapico et al., 2018)***. However, their function remains elusive. In particular, the presence of specific NK cell subsets within colon cancer and their potential relationship to CCLM progression have not been fully characterized to date.

In this study, we combined previously published single-cell RNA sequencing, spatial transcriptomics (ST), and bulk RNA-sequencing data from public datasets, aiming to comprehensively chart the cellular landscape of TME in primary colon cancer and matched liver metastasis. Results of bioinformatics analysis were further validated through an in vitro co-culture experiment (Fig. 1A).

Results

Integrated scRNA-seq and ST Precisely Quantified Immune Cell Diversity in CCLM

We used a previously published single-cell dataset containing 89 samples from paired samples of colon cancer, adjacent colon, liver metastasis, adjacent liver, lymph nodes along colons, and peripheral blood mononuclear cells from 20 patients to define the heterogeneous immune microenvironment landscapes of CCLM. Subsequently, 178,630 CD45+ cells were integrated.

To further define the main cell type, clustering analysis and SingleR were performed, and monocytes, neutrophil cells, native B cells, plasma cells, T cells, and NK cells were identified from the CCLM samples (Fig. 1B-C; Fig. S1A and B). Notably, T and NK cells were the major components of all immune cells and distinct across different tissue types, with NK cells significantly decreasing in tumor tissues (both primary colon cancer and liver metastasis cancer) compared to corresponding adjacent normal tissues, whereas T cells were the opposite (Fig. 1D and E; Fig. S1C).

To comprehensively analyze the spatial distribution profile of colon primary tumors and CCLM tumors, we collected ST data, which came from eight samples including paired primary colon cancer and liver metastasis. Unsupervised clustering analysis was first performed to cluster similar ST spots, and the annotation of the clusters was further determined according to cell marker genes (Fig. S2A-C). Further, after combining the gene expression features of each sample (Fig. S3) and H&E staining, six morphological regions, including tumor, fibroblast, smooth muscle, B cells, hepatocytes, normal epithelium, and tumor and paratumor areas, were identified. (Fig. 2A-C).

To integrate the scRNA-seq and ST data, we used the AddModuleScore function in Seurat to quantify the main immune subpopulations. Consistent with scRNA-seq, T cells were remarkably enriched in the tumor region of both primary colon cancer and liver metastasis cancer, whereas NK cells were enriched in the non-tumor area (Fig. 2D).

Biological Relationship Between NK Cells and Metastasis of Colon Cancer Revealed by Bulk RNA Transcriptomics

TME cell composition differences between metastasis and non-metastasis colon cancer were evaluated using multiple tools that could robustly quantify the abundance of cell populations based on transcriptomic datasets, including xCell, EPIC, quanTIseq, and MCPcounter and bulk-seq datasets (TCGA COAD cohort). The percentages of NK cells markedly decreased in metastasis colon cancer using MCPcounter, EPIC, and xCell (Fig. 3A-D).

To further understand the potential triggers that induce colon cancer metastasis, the DEGs were calculated between the metastasis and non-metastasis colon cancer groups in the TCGA COAD cohort. A total of 1,378 DEGs were determined using the limma package with cutoffs |log fold change|>1.5 and p <0.05, including 817 upregulated and 561 downregulated genes between metastasis and non-metastasis colon cancer (Fig. 3E). Subsequently, GO and KEGG enrichment analyses and GSEA were performed to investigate the correlative functions and pathways. As shown in Fig. 3F, cell killing, NK cell-mediated immunity, NK cell-mediated cytotoxicity, NK cell activation, and MHC-related GO terms were significantly enriched. The KEGG pathways of NK cell-mediated cytotoxicity were also enriched (Fig. 3F), with most of the genes in this pathway markedly downregulated in the metastasis group compared to the non-metastasis group. In contrast, GSEA revealed that NK cell-mediated cytotoxicity was enriched in the metastasis group (Fig. 3G and H).

The Landscape of NK Cells in CCLM Progression

The differences in infiltrated NK cells between tumor-adjacent tissues and tumor tissues suggest that the dynamic remodeling of NK cells may play an important role in CCLM progression. To further understand the landscape of NK cells in the CCLM microenvironments, NK cells were selected, and unsupervised clustering analysis was performed. Eight NK cell subtypes were thus identified (Fig. 4A). Combining the highly variable features of each NK cluster (Fig. 4B) and CIBERSORT-reported canonical NK cell markers (Fig. 4C and D), NK cells were classified into three cell types, including activated NK cells identified by the expression of KIR2DL4, GPR183, GRP171, CD69, and IFNG, resting NK cells marked by GZMK, TTC38, CD160, and PLEKNF1, and the other NK cells of which no characteristic gene was identified. Although all three NK cell subtypes were presented in primary colon tumors, adjacent normal colon tissues, liver metastasis tumors, and lymph nodes (Fig. 4E), the infiltration grade for each of these NK cell subsets was significantly different. At the individual sample level, considerable variability was observed in the NK cell subset composition. Where serial samples were available from individual patients, the expression of resting NK cells increased, whereas that of activated NK cells decreased during disease progression (Fig. 4F and G). Additionally, using the paired primary colon tumor, adjacent normal colon tissues, and liver metastasis tumor samples, we observed that the gradient of the resting NK cells increased, whereas the gradient of the activated NK cells decreased (Fig. 4H).

To evaluate the clinical relationship between NK cell differences and CCLM, CIBERSORT was performed using the TCGA COAD cohort. The percentages of resting NK cells significantly increased (Fig. 5A), and the activated NK cells decreased in the metastasis group (Fig. 5B), which is consistent with the scRNA-seq results. Also, we observed that the resting NK cells were significantly increased, whereas the activated NK cells decreased in higher T, N, and TNM stages (Fig. S4A). In terms of survival, neutrophils and resting NK cells were associated with a worse prognosis, whereas activated NK cells and M1 macrophages were associated with better outcomes (Fig. S4B). Further, survival analysis showed that colon cancer

patients with lower and higher degrees of infiltration of activated NK cells and resting NK cells, respectively, had a significantly worse prognosis in the TCGA COAD and GSE29623 cohorts (Fig. 5C and D). Interestingly, resting NK cells were remarkably enriched in the tumor region, whereas activated NK cells were enriched in the non-tumor area of both primary colon cancer and liver metastasis (Fig. 5E).

Characterization and Developmental Course of Differential Subsets of NK Cells in CCLM

To further study the heterogeneity of NK cells subgroup, the proportions of all eight clusters of NK cells were calculated (Fig. S5). KIR2DL4+ GPR171+ activated NK cells were lessened in proportion with the progression of the disease from normal colon to colon cancer and liver metastasis cancer, whereas GZMK+ resting NK cells increased (Fig. 6A and B), suggesting that these two NK subsets were associated with metastasis. ST analysis also confirmed that there was more infiltration of the KIR2DL4+ GPR171+ activated NK cell subset in the non-tumor area and GZMK+ resting NK cells in the tumor region, both primary colon cancer and liver metastasis (Fig. 6C).

Pseudotime cell trajectory analysis of the two NK cell clusters was constructed to investigate the evolutionary dynamics of metastasis-associated NK cells. NK cells from the normal colon group were located at the top right corner of the trajectory curve, suggesting the clear starting point of this evolving trajectory curve. After confirmation of this starting point, developmental routes were determined to begin with the KIR2DL4+ GPR171+ activated NK cells and then develop into GZMK+ resting NK cells (Fig. 6D).

To explore the transitional relationships of marker genes in NK cells in distinct clusters, we examined the expression level of these markers in different clusters through pseudotime analysis. Marker genes of activated NK cells (KIR2DL4 and GPR171) exhibited a gradient descent expression pattern, whereas the expression of resting NK cell marker genes (GZMK) exhibited a gradient rise pattern (Fig. 6E). BEAM analysis was performed to identify the cell cluster marker genes that change as NK cell subtypes move from the activated stage to the resting stage. The branched heatmap showed the expression dynamics of the top 200 significant genes in different cell fate branches. Corresponding GO enrichment analyses of these significant genes further demonstrated that a mass of leukocyte differentiation and immune system process-related GO terms were significantly enriched (Fig. 6F).

Interestingly, patients with colon cancer with higher infiltration of GZMK+ resting NK cells (Fig. 6G) and lower infiltration of KIR2DL4+ GPR171+ activated NK cells (Fig. 6H) exhibited shorter survival in the TCGA COAD cohort.

Tumor Cells-Educated NK Cells Shift Toward Tumor-Promoting Status Depends on Cell-to-Cell Interaction

Given the characteristic spatial distribution of NK cell subpopulations, we hypothesized that the tumor region-enriched NK cells might be educated by tumor cells and thus functionally distinct. To verify the possible effect of tumor cells on the

phenotypic switch of NK cells, we set up mixed cell co-culture experiments using colon cell line HCT-116 and NK cell line NK-92 in the ratio 1:1. As controls, NK cells were cultured alone, either in the tumor supernatant or fresh medium (Fig. S6A). After 24 h of co-culturing, NK cells were analyzed using FACS to determine the expression of the NK cells markers above identified as well as functional receptors NKG2A and NKG2D. Upon exposure to tumor cells, NK cells significantly decreased the expression of activated receptor KIR2DL4 (Fig. 7A) and functional receptors, both NKG2A and NKG2D (Fig. 7 B). However, no such effect was observed after co-culturing with tumor supernatant and fresh medium.

To explore the NK cell-mediated inductive effect on colon cells, we performed co-culture experiments in transwells, and the co-cultured supernatant was collected to incubate fresh HCT-116 (Fig. S6B).

Interestingly, HCT-116 cells in the CNS group underwent a significant increase in proliferation (Fig. 7C-E) and migration (Fig. 7F-H) compared to the CS group, where cancer cells were cultured directly in the supernatant after 24 h of cancer cell culturing. Furthermore, CCK-8 (Fig. 7I) and colony formation assays (Fig. 7J-K) showed that colon cells underwent a significant increase in proliferation when cultured in the supernatant from the co-culture system in which NK and colon cells were in contact (CNS group), but not when co-cultures were performed in the cell supernatant (SNS group) and fresh medium (MNS group). Similarly, the migration and invasion of HCT-116 were significantly increased when cultured in the supernatant from the co-culture system in which NK and colon cells were in contact (CNS group) (Fig. 7L-N).

Further, another colon cancer cell line, DLD-1, was chosen to evaluate the effect of the supernatant in the different co-culture groups. DLD-1 cells in the CNS group did not undergo a prominent increase in proliferation, as HCT-116 and CCK-8 assays showed a minimal proliferation of colon cells in the MNS group (Fig. S7A-C). The same results were obtained for their migration and invasion (Fig. S7D-F). However, no such cell functional changes were induced in the CNS group (Fig. S7G-L).

Resting NK-induced Colon Cancer Malignant Phenotype Promotion Depends on SCF Release

To study the potential mechanism by which the supernatant from the NK and colon cells in direct contact with the co-culture system promoted colon cell migration, Luminex liquid suspension chip detection was used to compare the differential expression of 48 common chemotactic and inflammatory cytokines in the CNS, SNS, and MNS groups. We observed that SCF was upregulated in all three repetitions in the CNS group (Fig. 8A-B). Further, ELISA confirmed the upregulated level of SCF in the CNS group (Fig. 8C).

We further assessed the inhibitory effects of imatinib mesylate on the enhanced proliferation and invasion. CCK-8 (Fig. 8D-E) and colony formation assays (Fig. 8F-I) showed that imatinib mesylate (2 μM) significantly inhibited supernatant-enhanced proliferation of HCT-116. Similarly, the supernatant-enhance migration (Fig. 8J-K) and invasion (Fig. 8L-M) were also inhibited by imatinib.

Discussion

CCLM is a multistep process and is mostly fatal***(Manfredi et al., 2006)***. During disease progression**,** functional interactions between tumor cells and the surrounding TME are critical for influencing tumor growth, promoting angiogenesis, and finally resulting in metastasis***(Quail et al., 2013)***. Since the genomic divergence between primary and metastatic CRC cells is relatively low***(Wei et al., 2017, Yaeger et al., 2018)*** and accumulating evidence has highlighted the key role of tumor-infiltrating immune cells in dictating the fate of cancer cells***(Kumar et al., 2018, Hanahan et al., 2012)***, we presented a comprehensive cellular and spatial immune landscape of the primary and liver metastatic tumors of CRC by using previously published scRNA-seq and ST data. Consistent with previous studies***(Zhou et al., 2021, Wu et al., 2022)***, we observed that the immune microenvironment of primary and liver metastasis lesions of colon cancer had undergone extensive remodeling with a significantly decreased proportion of NK cells and a strong enrichment of T cells. However, the contrast between the decreased proportion of NK cells in tumor tissue and the enrichment of NK cells in tumor regions may indicate the specific effects of NK cells in CCLM.

Traditionally, NK cells within the TME were known as potential suppressors for tumor growth by directly killing cells and secreting proinflammatory cytokines***(Huntington et al., 2007, Freud et al., 2006)***. However, the function of NK cells highly depends on their maturation status and localization***(Cooper et al., 2001)***. The peripheral blood $CD56^{dim}CD16^{high}$ NK cell population predominantly mediates the killing of target cells by secreting perforin and granzymes***(Jacobs et al., 2001)***, whereas the $CD56^{bright}CD16^{low}$ NK cells that reside in secondary lymphoid tissues are immature and have reduced cytotoxic capability***(Moretta, 2010)***. Recently, tumor-associated NK cells, which are enriched in tumors with impaired anti-tumor functions, were discovered to be associated with an unfavorable prognosis and resistance to immunotherapy in multiple solid tumors ***(Tang et al., 2023)***, such as lung cancer, pancreatic cancer, and esophageal cancer. The potential impact of NK cells on CCML progression is still poorly investigated.

In this study, the proportion of NK cells was higher than in past cognition, similar to a previous study***(Xia et al., 2022)*** in that NK cells occupied the largest immune cell compartment of nearly 50% in cholangiocarcinoma. In contrast, NK cells may not be well distinguished during automatic annotation using SingleR. Consistent with the study that revealed that treatment responders are associated with TME remodeling, including NK cell recruitment***(Kim et al., 2022)***, the proportions of NK cells in PR patients were significantly higher among the LiverP and LiverT groups (Fig. S1D and E), which also increased the overall proportion of NK cells to some extent. Additionally, we observed that NK cells are decreased in primary colon cancer and liver metastatic using scRNA-seq, consistent with previous findings supporting that NK cells play a crucial role in anticancer immunity***(Laskowski et al., 2022, Myers et al., 2021)***. However, we further subdivided NK cells considering the conflicting result, in which NK cells were significantly enriched in the tumor area

when using ST. Since this is the first study to comprehensively explore the heterogeneity of NK cells, no previous NK cell subpopulation markers were available; resting and activated NK cell markers in CIBERSORT were thus used to annotate NK cells. Consistent with a recent study that reported that mature and immature NK cells serve different functions***(Thacker et al., 2023)***, our results also provide evidence that resting NK cells in the colon cancer TME possess a potential tumor-promoting activity, whereas activated NK cells play an anti-tumor role as conventional cognition. Bulk RNA-sequencing and the corresponding clinical data further indicated that higher infiltration of resting NK cells and lower infiltration of activated NK cells were correlated with a worse prognosis in patients with CRC. However, since the resting and activated NK cells we identified were only the aggregation of multiple NK cell subpopulations, further studies are required to investigate the key NK cell subpopulations that play a crucial role in CCLM.

Further analysis of NK cell subtypes revealed a dramatic change in KIR2DL4+ GPR171+ activated NK cells and GZMK+ resting NK cells, whereas no other NK cell subpopulations differed in colon cancer progression. KIR2DL4, also known as CD158d, is an unusual member of the killer cell Ig-like receptor family expressed in all NK cells***(Andre et al., 2001)***. Studies revealed that KIR2DL4 activates the cytotoxicity of NK cells***(Faure et al., 2002)***, and NK-92 cells stimulated with KIR2DL4 had higher cytotoxicity against breast cancer cells***(Kilic et al., 2023)***. Consistent with previous studies, we also observed that the expression of the KIR2DL4+ GPR171+ activated NK cell subtype was decreased during CCLM progression, possibly reflecting the anti-tumor activity of this population. However, the GZMK+ resting NK cell subsets were first identified as potential tumor promoters. Moreover, it has been proven that $GZMK^{high}$ $CD8^{+}$ T effector memory cells, a cell subset that is particularly similar to GZMK+ NK cells, were associated with poor clinical outcomes in patients with colorectal tumors. Our results also showed that GZMK+ resting NK cells highly infiltrate the cancer region, and this predicts a worse prognosis in patients with colon cancer. However, despite the interesting and gratifying clinical relevance, the mechanism remains unknown.

Considering the evolutionary trajectory and the characteristic distribution of these metastasis-associated NK cell subtypes, we predicted that activated NK cells might differentiate into resting NK cells under the action of tumor cells. Consistent with a recent study that indicated that exposure to cancer cells causes NK cells to lose their cytotoxic ability***(Chan, Knutsdottir, 2020)***, we identified the tendency of NK cells to differentiate to an resting state with decreasing expression of activated marker KIR2DL4 as well as typical functional NK cell markers: NKG2D***(Yu et al., 2023)*** and NKG2A which are only triggered by cell-to-cell interactions as validated by FACS. Unfortunately, resting markers GZMK can not be detected in all the three groups since it's a secreted protein.

Additionally, NK-mediated tumor cell editing appears to partly depend on the release of cytokines in in vitro co-culture experiments. SCF, the natural ligand of c-Kit with membrane-bound (mSCF) and soluble forms (sSCF)***(Hsu et al., 1997)***, enhances the growth and migration of cancer cells such as cervical cancer***(Aguilar et***

387 ***al., 2014)***, Ewing's sarcoma***(Landuzzi et al., 2000)*** and CRC***(Yasuda et al., 2007)***.
388 Although the dimeric mSCF is remarkably more active and induces a more persistent
389 activation of the receptor***(Hsu, Wu, 1997, Langley et al., 1993)***, the tumor-promoting
390 effect of the supernatant from the co-culture system in the current study and the
391 reversion effect of imatinib for the co-culture supernatant induced pro-oncogenic
392 effects suggests an important role of sSCF on colon cancer cells. However, no up-
393 regulation of KITLG (the SCF encoding gene) was found in HCT-116 after co-
394 culturing with NK cells (Fig. S9A). In addition, when using DLD-1, a colon cancer
395 cell with a nearly 15 times lower expression of KITLG than HCT-116 (Fig. S9B), we
396 also did not observe co-cultured supernatant induced tumor-promoting effects. We
397 thus hypothesized that in our experimental system, NK cells may promote the
398 cleavage and release of the extracellular part of SCF on the tumor cell surface after
399 direct contact with tumor cells, and thus increase the concentration of sSCF, which
400 induces the malignant phenotype of colon cancer cells in a paracrine manner (Fig. 8J).
401 However, the detailed mechanism still needs to be further studied.
402 In summary, we have unveiled the spatial and cellular profiles of TME from
403 tumors and paratumor tissues of CCLM. Our analysis uncovered the different states,
404 functions, and dynamic nature of NK cells in different CCLM settings, which can be
405 used for further identification of regulatory mechanisms and for developing potential
406 therapeutic targets.
407
408 **Materials and Methods**
409 **Single-cell RNA Sequencing Analysis**
410 The R (v4.0.5) package Seurat (v4.1.0)***(Hao et al., 2021)*** was used to process the
411 scRNA data. Since dataset quality control had been performed and Seurat objects had
412 been created in previous studies, we did not further filter the scRNA-seq data or
413 remove the batch effects. The SCTransform method was used to normalize the data.
414 After selecting 2,000 highly variable genes using the Find Variable Features function
415 in Seurat, principal component analysis was performed using these genes to reduce
416 the data dimensions. Based on the ElbowPlot function in Seurat, we chose the top 30
417 principal components to run the FindNeighbors function. Next, the cells were
418 clustered using the FindClusters function with a resolution of 0.1 for clustering
419 immune cells. A uniform manifold approximation and projection algorithm was used
420 for data visualization, as previously reported***(Peng et al., 2023)***. Differentially
421 expressed genes (DEGs) of each subset were identified using the FindAllMarkers
422 function in Seurat. SingleR (v1.0.0) was used to name each cluster***(Zheng et al.,***
423 ***2021)***.
424
425 **Pseudotime Analysis**
426 To analyze the differentiations of NK cells, monocle2 (http://cole-trapnell-
427 lab.github.io/monocle-release), which uses an algorithm to learn the changes in gene
428 expression sequences that each cell must undergo as part of a dynamic biological
429 process***(Hong et al., 2022)***, was used for pseudotime trajectory analysis to identify the
430 transitional relationships among different clusters. The cells were reduced

dimensionally using the DDRTree method, sequenced in pseudotime, and finally visualized***(Qiu et al., 2017)***.

Bulk RNA-seq Data Analysis

The bulk transcriptome RNA-seq data and corresponding clinical data were obtained from The Cancer Genome Atlas of colon adenocarcinoma through the UCSC Xena browser (GDC hub) (https://gdc.xenahubs.net)***(Goldman et al., 2020)***. In total, 459 colon cancer samples with survival information were downloaded, and 310 samples were finally enrolled (11 formalin-fixed samples were excluded, and an additional 134 and 4 samples were excluded due to deletion of metastasis information and sequencing matrix, respectively). Transcriptomic data from 65 colon cancer samples in GSE29623 were obtained as the validation cohorts. CIBERSORT***(Chen et al., 2018)***, xCELL***(Aran et al., 2017)***, EPIC***(Racle et al., 2017)***, and MCP-counter***(Becht et al., 2016)***, which use gene expression to infer the proportions of tumor-infiltrating immune cells, were used to analyze the TME cell type. R packages survival (v3.2-10) and survminer (v0.4.9) were used for survival analysis. The Youden index was selected as the cutoff value to differentiate patients into distinct groups (high or low). The Kaplan–Meier survival curve was modeled using the survfit function. Subsequently, a Cox proportional hazards regression model was established to determine the independent risk factors. DEGs between the metastasis and non-metastasis groups were determined with the filtering condition of log2 |fold change|>1 and p-value <0.05, using the R package limma. GO and KEGG pathway functional enrichment analyses were performed using the clusterProfiler R package (v3.18.1) to assign various biological processes, molecular functions, cellular components, and pathways of identified marker genes in the cluster of interest***(Yu et al., 2012)***, and p <0.05 was regarded as statistically enriched. To explore the different KEGG pathways and hallmark gene sets between the metastasis and non-metastasis groups, gene set enrichment analysis (GSEA) was performed using data from The Molecular Signatures Database (c2.cp.kegg.v7.3.symbols) and the fgsea R package (v1.12.0)***(Liberzon et al., 2015)***. Pathways with an adjusted p-value below 0.05 were deemed to be significantly enriched.

ST Data Analysis

Seurat was also used for ST data processing and visualization. We used the SCT method to normalize the ST data; the functions SelectIntegrationFeatures, PrepSCTIntegration, FindIntegrationAnchors, and IntegrateData were used to integrate the ST data. An unsupervised clustering method was subsequently used to cluster similar ST spots. Cell population annotations were based on hematoxylin and eosin (H&E) staining sections and the highly variable genes in each cluster. Scores of cell-specific signatures (top 20 DEGs) from scRNA-seq were calculated using the AddModuleScore function. SpatialDimPlot and SpatialFeaturePlot were combined to visualize the cell expression level in the ST data***(Peng, Ren, 2023)***.

Cell Lines and Co-cultures

Colon carcinoma cell lines HCT-116 and DLD-1 were purchased from the Cell Bank of the Chinese Academy of Sciences (Shanghai, China) and grown in a RPMI-1640 medium (GIBCO/BRL) supplemented with 10% FBS (GIBCO/BRL) in a humidified chamber at 37 °C and 5% CO_2. The human NK cell line NK-92 was also purchased from the Cell Bank of the Chinese Academy of Sciences (Shanghai, China) and maintained in RPMI-1640 supplemented with 12.5% horse serum (GIBCO), 12.5% FBS, 100 U/mL rhIL-2, 0.1 mmol/L b-mercaptoethanol, and 0.02 mmol/L folic acid.

Colon cancer cells were plated at a density of 1×10^5 cells/well in 6-well plates for 24 h. Supernatants were collected, and cells and debris were removed by centrifugation. NK cells were co-cultured with cancer cells in a ratio of 1:1 in a fresh mixed medium for a further 24 h. Additionally, NK cells were cultured in the soluble supernatant for 24 h with a supernatant/RPMI-1640 10% FBS and NK medium in the ratio 1:1. When indicated, co-cultures were performed in Transwell devices (JET biofil), maintaining the same ratios and culture times.

Flow Cytometry Analysis

NK cells in each co-cultured group were collected and washed twice in 1 × PBA. Then, they were incubated with PE-labeled KIR2DL4 (Affinity Biosciences), FITC-labeled GZMK(Affinity Biosciences), FITC-labeled NKG2A (Biolegend) and PE-labeled NKG2D antibody (Biolegend) for 30 min, rewashed, and resuspended in PBS. BD flow cytometry was used for detection.

Cell Counting Kit-8 (CCK-8) Cell Viability and Cell Colony Formation Assay

Colon cancer cells (5,000 cells/well) were cultured in 96-well plates with with co-cultured supernatants from different co-culture groups alone or with both co-cultured supernatants and imatinib mesylate (2 μM) as previously reported***(Yasuda, Sawai, 2007)*** for 24 h. At pre-determined time points, 10 μL of CCK-8 reagent (Dojindo, Japan) was added and incubated for 2 h at 37 °C, and then the absorbance was measured using a microplate reader (Thermo Scientific) at 450 nm. All experiments were carried out in triplicate.

For the cell colony formation assay, colon cancer cells (500 cells/well) were seeded in 12-well plates with co-cultured supernatants alone or with both co-cultured supernatants and imatinib mesylate at 37 °C for 1 week. Then, cell colonies were fixed with 4% paraformaldehyde for 10 min and stained with 0.5% crystal violet for 5 min. Cell colonies containing >20 cells were counted. All experiments were carried out in triplicate.

Transwell Migration/Invasion Assays

The polycarbonate membrane in the transwell chambers was coated with Matrigel (Corning, NY, USA). Next, we transferred 1×10^5 cells from the serum-free medium with or without imatinib mesylate into the top chamber, added co-cultured supernatants alone or with both co-cultured supernatants and imatinib mesylate in the bottom chamber, and incubated at 37 °C for 24 h. Then, we removed the non-invading

cells on the top side of the membrane by scrubbing, fixed the migrating or invading cells at the bottom side of the membrane with 4% paraformaldehyde, and stained with 0.5% crystal violet. The number of cells was counted under a microscope (Leica, London, UK) from four randomly chosen fields per well to determine the number of cells in each group.

Total RNA Extraction and Quantitative Real-Time PCR (qPCR)

Total RNA was extracted from cells using TRIZOL reagent (Invitrogen, USA). RNA was reverse transcribed into cDNA using a PrimeScript RT Reagent Kit (Takara, Japan). qPCR was performed using QuantStudio™ Test Development Software (Thermo Scientific, Waltham, MA, USA) with SYBR Green qPCR Master Mix (EZBioscience, Roseville, MN, USA). The sequence of KITLG and housekeeping gene GAPDH primers is listed in Table S1. KITLG mRNA data were normalized to that of GAPDH.

Luminex Liquid Suspension Chip Detection and ELISA

Luminex liquid suspension chip detection was performed by Wayen Biotechnologies (Shanghai, China). The Bio-Plex Pro Human Chemokine Panel 48-plex kit was used in accordance with the manufacturer's instructions. Briefly, supernatants from different co-cultured groups were incubated in 96-well plates embedded with microbeads for 1 h and then incubated with a detection antibody for 30 min. Subsequently, streptavidin-PE was added in each well for 10 min, and values were read using the BioPlex MAGPIX System (Bio-Rad). The Human SCF ELISA kit (Solarbio, China) was used according to the manufacturer's instructions.

Statistical Analysis and Visualization

All statistical analyses were performed using SPSS (v23.0; IBM SPSS, Chicago, IL, USA) and R (v4.0.5), and data visualization was performed on R packages Seurat (v4.1.0), ggplot2 (v3.3.5), ggsignif (v0.6.1), and pheatmap (v1.0.12).

Data Availability

The raw data of single-cell RNA sequencing and ST data (10X Genomics) were derived from previously published research at the website: http://www.cancerdiversity.asia/scCCLM/)***(Wu, Yang, 2022)***. And two bulk transcriptomics data of colon cancer were downloaded from TCGA cohort COAD at the website: https://xena.ucsc.edu/ and NCBI's Gene Expression Omnibus with accession number GSE29623. All data generated or analyzed during this study are available from the corresponding author on reasonable request.

Funding

Funder	Grant reference number	Author
National Natural Science Foundation of China	32070151	Xian Shen
Key R&D Program of	2020C03029	Xiangyang Xue

Zhejiang Province		
Key R&D Program of Zhejiang Province	2021C03120	Xian Shen
the Zhejiang Provincial Natural Science Foundation Project	Q24H160147	Wangkai Xie
the Postdoctoral Fellowship Program of CPSF	GZC20231956	Wangkai Xie
the Wenzhou Municipal Science and Technology Bureau Program	Y2020215	Dan Xiang
The funders had no role in study design, data collection and interpretation, or the decision to submit the work for publication		

Acknowledgement

We thank Prof. Qiang Gao from Fudan University and Prof. Xiaoming Zhang from Shanghai Institute of Immunity and Infection, CAS for sharing the SC RNA sequencing and ST data. We thank Zhejiang Key Laboratory of New Techniques for Diagnosis and Treatment of Critical Diseases of Pancreas and Liver and Zhejiang International science and Technology Cooperation base for tumor transformation research for supporting this study. We thank Editage Group (https://www.editage.cn/) for polishing the draft of this manuscript.

]

Authors' Contributions:

CCM and **YYC**: Conceptualization, experimental design and execution, data curation, method development, formal analysis, statistics, writing original draft, and editing the manuscript. **DX** and **TMZ**: conceptualization, data curation and method development. **DFM** and **ZH**: experimental design. **WKX** and **CL**: experimental design. **YXL** and **JYY**: Validation. **DX**, **MDL** and **XYX**: Experimental design, supervision, funding acquisition, and manuscript editing. **XS**: Conceptualization, supervision, writing manuscript, project administration.

References

1. Sung H, Ferlay J, Siegel RL, Laversanne M, Soerjomataram I, Jemal A, Bray F. 2021. Global Cancer Statistics 2020: GLOBOCAN Estimates of Incidence and Mortality Worldwide for 36 Cancers in 185 Countries. CA Cancer J Clin.71:209-49. DOI: https://doi.org/10.3322/caac.21660, PMID: 33538338.
2. Siegel RL, Miller KD, Goding Sauer A, Fedewa SA, Butterly LF, Anderson JC, Cercek A, Smith RA, Jemal A. 2020. Colorectal cancer statistics, 2020. CA Cancer J Clin.70:145-64. DOI: https://doi.org/10.3322/caac.21601, PMID: 32133645.
3. Wang F, Long J, Li L, Wu ZX, Da TT, Wang XQ, Huang C, Jiang YH, Yao XQ, Ma HQ, Lian ZX, Zhao ZB, Cao J. 2023. Single-cell and spatial transcriptome analysis reveals the cellular heterogeneity of liver metastatic colorectal cancer. Sci Adv.9:eadf5464. DOI: https://doi.org/10.1126/sciadv.adf5464, PMID: 37327339.
4. Chua TC, Saxena A, Chu F, Zhao J, Morris DL. 2011. Predictors of cure after hepatic resection of colorectal liver metastases: an analysis of actual 5- and 10-year survivors. J Surg Oncol.103:796-800. DOI: https://doi.org/10.1002/jso.21864, PMID: 21246567.
5. Zampino MG, Magni E, Ravenda PS, Cella CA, Bonomo G, Della Vigna P, Galdy S, Spada F, Varano GM, Mauri G, Fazio N, Orsi F. 2016. Treatments for colorectal liver metastases: A new focus on a familiar concept. Crit Rev Oncol Hematol.108:154-63. DOI: https://doi.org/10.1016/j.critrevonc.2016.11.005, PMID: 27931834.
6. Ruers T, Van Coevorden F, Punt CJ, Pierie JE, Borel-Rinkes I, Ledermann JA, Poston G, Bechstein W, Lentz MA, Mauer M, Folprecht G, Van Cutsem E, Ducreux M, Nordlinger B, European Organisation for R, Treatment of C, Gastro-Intestinal Tract Cancer G, Arbeitsgruppe Lebermetastasen und tumoren in der Chirurgischen Arbeitsgemeinschaft O, National Cancer Research Institute Colorectal Clinical Study G. 2017. Local Treatment of Unresectable Colorectal Liver Metastases: Results of a Randomized Phase II Trial. J Natl Cancer Inst.109. DOI: https://doi.org/10.1093/jnci/djx015, PMID: 28376151.
7. Wancata LM, Banerjee M, Muenz DG, Haymart MR, Wong SL. 2016. Conditional survival in advanced colorectal cancer and surgery. J Surg Res.201:196-201. DOI: https://doi.org/10.1016/j.jss.2015.10.021, PMID: 26850202.
8. Piawah S, Venook AP. 2019. Targeted therapy for colorectal cancer metastases: A review of current methods of molecularly targeted therapy and the use of tumor biomarkers in the treatment of metastatic colorectal cancer. Cancer.125:4139-47. DOI: https://doi.org/10.1002/cncr.32163, PMID: 31433498.
9. Yao J, Chen Y, Lin Z. 2023. Exosomes: Mediators in microenvironment of colorectal cancer. Int J Cancer.153:904-17. DOI: https://doi.org/10.1002/ijc.34471, PMID: 36760212.
10. Liu H, Wang Z, Zhou Y, Yang Y. 2023. MDSCs in breast cancer: an important enabler of tumor progression and an emerging therapeutic target. Front Immunol.14:1199273. DOI: https://doi.org/10.3389/fimmu.2023.1199273, PMID: 37465670.
11. Ngambenjawong C, Gustafson HH, Pun SH. 2017. Progress in tumor-associated macrophage (TAM)-targeted therapeutics. Adv Drug Deliv Rev.114:206-21. DOI: https://doi.org/10.1016/j.addr.2017.04.010, PMID: 28449873.
12. Li S, Cong X, Gao H, Lan X, Li Z, Wang W, Song S, Wang Y, Li C, Zhang H, Zhao Y, Xue Y. 2019. Tumor-associated neutrophils induce EMT by IL-17a to promote migration and invasion in gastric cancer cells. J Exp Clin Cancer Res.38:6. DOI: https://doi.org/10.1186/s13046-018-1003-0,

622 PMID: 30616627.
623 13. Tiberti S, Catozzi C, Croci O, Ballerini M, Cagnina D, Soriani C, Scirgolea C, Gong Z, He J,
624 Macandog AD, Nabinejad A, Nava Lauson CB, Quinte A, Bertalot G, Petz WL, Ravenda SP, Licursi V,
625 Paci P, Rasponi M, Rotta L, Fazio N, Ren G, Fumagalli-Romario U, Schaefer MH, Campaner S, Lugli
626 E, Nezi L, Manzo T. 2022. GZMK(high) CD8(+) T effector memory cells are associated with
627 CD15(high) neutrophil abundance in non-metastatic colorectal tumors and predict poor clinical
628 outcome. Nat Commun.13:6752. DOI: https://doi.org/10.1038/s41467-022-34467-3, PMID: 36347862.
629 14. Maskalenko NA, Zhigarev D, Campbell KS. 2022. Harnessing natural killer cells for cancer
630 immunotherapy: dispatching the first responders. Nat Rev Drug Discov.21:559-77. DOI:
631 https://doi.org/10.1038/s41573-022-00413-7, PMID: 35314852.
632 15. Zhong F, Lin Y, Jing X, Ye Y, Wang S, Shen Z. 2022. Innate tumor killers in colorectal cancer.
633 Cancer Lett.527:115-26. DOI: https://doi.org/10.1016/j.canlet.2021.12.022, PMID: 34952144.
634 16. Villegas FR, Coca S, Villarrubia VG, Jimenez R, Chillon MJ, Jareno J, Zuil M, Callol L. 2002.
635 Prognostic significance of tumor infiltrating natural killer cells subset CD57 in patients with squamous
636 cell lung cancer. Lung Cancer.35:23-8. DOI: https://doi.org/10.1016/s0169-5002(01)00292-6, PMID:
637 11750709.
638 17. Ishigami S, Natsugoe S, Tokuda K, Nakajo A, Che X, Iwashige H, Aridome K, Hokita S, Aikou T.
639 2000. Prognostic value of intratumoral natural killer cells in gastric carcinoma. Cancer.88:577-83. DOI:
640 PMID: 10649250.
641 18. Lamb MG, Rangarajan HG, Tullius BP, Lee DA. 2021. Natural killer cell therapy for hematologic
642 malignancies: successes, challenges, and the future. Stem Cell Res Ther.12:211. DOI:
643 https://doi.org/10.1186/s13287-021-02277-x, PMID: 33766099.
644 19. Liu E, Marin D, Banerjee P, Macapinlac HA, Thompson P, Basar R, Nassif Kerbauy L, Overman
645 B, Thall P, Kaplan M, Nandivada V, Kaur I, Nunez Cortes A, Cao K, Daher M, Hosing C, Cohen EN,
646 Kebriaei P, Mehta R, Neelapu S, Nieto Y, Wang M, Wierda W, Keating M, Champlin R, Shpall EJ,
647 Rezvani K. 2020. Use of CAR-Transduced Natural Killer Cells in CD19-Positive Lymphoid Tumors. N
648 Engl J Med.382:545-53. DOI: https://doi.org/10.1056/NEJMoa1910607, PMID: 32023374.
649 20. Zhang H, Yang L, Wang T, Li Z. 2024. NK cell-based tumor immunotherapy. Bioact Mater.31:63-
650 86. DOI: https://doi.org/10.1016/j.bioactmat.2023.08.001, PMID: 37601277.
651 21. Hu W, Wang G, Huang D, Sui M, Xu Y. 2019. Cancer Immunotherapy Based on Natural Killer
652 Cells: Current Progress and New Opportunities. Front Immunol.10:1205. DOI:
653 https://doi.org/10.3389/fimmu.2019.01205, PMID: 31214177.
654 22. Oh S, Lee JH, Kwack K, Choi SW. 2019. Natural Killer Cell Therapy: A New Treatment
655 Paradigm for Solid Tumors. Cancers (Basel).11. DOI: https://doi.org/10.3390/cancers11101534, PMID:
656 31614472.
657 23. Bruno A, Focaccetti C, Pagani A, Imperatori AS, Spagnoletti M, Rotolo N, Cantelmo AR, Franzi
658 F, Capella C, Ferlazzo G, Mortara L, Albini A, Noonan DM. 2013. The proangiogenic phenotype of
659 natural killer cells in patients with non-small cell lung cancer. Neoplasia.15:133-42. DOI:
660 https://doi.org/10.1593/neo.121758, PMID: 23441128.
661 24. Carrega P, Morandi B, Costa R, Frumento G, Forte G, Altavilla G, Ratto GB, Mingari MC,
662 Moretta L, Ferlazzo G. 2008. Natural killer cells infiltrating human nonsmall-cell lung cancer are
663 enriched in CD56 bright CD16(-) cells and display an impaired capability to kill tumor cells.
664 Cancer.112:863-75. DOI: https://doi.org/10.1002/cncr.23239, PMID: 18203207.
665 25. Zhang QF, Yin WW, Xia Y, Yi YY, He QF, Wang X, Ren H, Zhang DZ. 2017. Liver-infiltrating

666 CD11b(-)CD27(-) NK subsets account for NK-cell dysfunction in patients with hepatocellular
667 carcinoma and are associated with tumor progression. Cell Mol Immunol.14:819-29. DOI:
668 https://doi.org/10.1038/cmi.2016.28, PMID: 27321064.
669 26. Jin J, Fu B, Mei X, Yue T, Sun R, Tian Z, Wei H. 2013. CD11b(-)CD27(-) NK cells are associated
670 with the progression of lung carcinoma. PLoS One.8:e61024. DOI:
671 https://doi.org/10.1371/journal.pone.0061024, PMID: 23565296.
672 27. Chan IS, Knutsdottir H, Ramakrishnan G, Padmanaban V, Warrier M, Ramirez JC, Dunworth M,
673 Zhang H, Jaffee EM, Bader JS, Ewald AJ. 2020. Cancer cells educate natural killer cells to a
674 metastasis-promoting cell state. J Cell Biol.219. DOI: https://doi.org/10.1083/jcb.202001134, PMID:
675 32645139.
676 28. Huergo-Zapico L, Parodi M, Cantoni C, Lavarello C, Fernandez-Martinez JL, Petretto A,
677 DeAndres-Galiana EJ, Balsamo M, Lopez-Soto A, Pietra G, Bugatti M, Munari E, Marconi M, Mingari
678 MC, Vermi W, Moretta L, Gonzalez S, Vitale M. 2018. NK-cell Editing Mediates Epithelial-to-
679 Mesenchymal Transition via Phenotypic and Proteomic Changes in Melanoma Cell Lines. Cancer
680 Res.78:3913-25. DOI: https://doi.org/10.1158/0008-5472.CAN-17-1891, PMID: 29752261.
681 29. Manfredi S, Lepage C, Hatem C, Coatmeur O, Faivre J, Bouvier AM. 2006. Epidemiology and
682 management of liver metastases from colorectal cancer. Ann Surg.244:254-9. DOI:
683 https://doi.org/10.1097/01.sla.0000217629.94941.cf, PMID: 16858188.
684 30. Quail DF, Joyce JA. 2013. Microenvironmental regulation of tumor progression and metastasis.
685 Nat Med.19:1423-37. DOI: https://doi.org/10.1038/nm.3394, PMID: 24202395.
686 31. Wei Q, Ye Z, Zhong X, Li L, Wang C, Myers RE, Palazzo JP, Fortuna D, Yan A, Waldman SA,
687 Chen X, Posey JA, Basu-Mallick A, Jiang BH, Hou L, Shu J, Sun Y, Xing J, Li B, Yang H. 2017.
688 Multiregion whole-exome sequencing of matched primary and metastatic tumors revealed genomic
689 heterogeneity and suggested polyclonal seeding in colorectal cancer metastasis. Ann Oncol.28:2135-41.
690 DOI: https://doi.org/10.1093/annonc/mdx278, PMID: 28911083.
691 32. Yaeger R, Chatila WK, Lipsyc MD, Hechtman JF, Cercek A, Sanchez-Vega F, Jayakumaran G,
692 Middha S, Zehir A, Donoghue MTA, You D, Viale A, Kemeny N, Segal NH, Stadler ZK, Varghese AM,
693 Kundra R, Gao J, Syed A, Hyman DM, Vakiani E, Rosen N, Taylor BS, Ladanyi M, Berger MF, Solit
694 DB, Shia J, Saltz L, Schultz N. 2018. Clinical Sequencing Defines the Genomic Landscape of
695 Metastatic Colorectal Cancer. Cancer Cell.33:125-36 e3. DOI:
696 https://doi.org/10.1016/j.ccell.2017.12.004, PMID: 29316426.
697 33. Kumar S, Wilkes DW, Samuel N, Blanco MA, Nayak A, Alicea-Torres K, Gluck C, Sinha S,
698 Gabrilovich D, Chakrabarti R. 2018. DeltaNp63-driven recruitment of myeloid-derived suppressor
699 cells promotes metastasis in triple-negative breast cancer. J Clin Invest.128:5095-109. DOI:
700 https://doi.org/10.1172/JCI99673, PMID: 30295647.
701 34. Hanahan D, Coussens LM. 2012. Accessories to the crime: functions of cells recruited to the
702 tumor microenvironment. Cancer Cell.21:309-22. DOI: https://doi.org/10.1016/j.ccr.2012.02.022,
703 PMID: 22439926.
704 35. Zhou SN, Pan WT, Pan MX, Luo QY, Zhang L, Lin JZ, Zhao YJ, Yan XL, Yuan LP, Zhang YX,
705 Yang DJ, Qiu MZ. 2021. Comparison of Immune Microenvironment Between Colon and Liver
706 Metastatic Tissue in Colon Cancer Patients with Liver Metastasis. Dig Dis Sci.66:474-82. DOI:
707 https://doi.org/10.1007/s10620-020-06203-8, PMID: 32193860.
708 36. Wu Y, Yang S, Ma J, Chen Z, Song G, Rao D, Cheng Y, Huang S, Liu Y, Jiang S, Liu J, Huang X,
709 Wang X, Qiu S, Xu J, Xi R, Bai F, Zhou J, Fan J, Zhang X, Gao Q. 2022. Spatiotemporal Immune

Landscape of Colorectal Cancer Liver Metastasis at Single-Cell Level. Cancer Discov.12:134-53. DOI: https://doi.org/10.1158/2159-8290.CD-21-0316, PMID: 34417225.

37. Huntington ND, Vosshenrich CA, Di Santo JP. 2007. Developmental pathways that generate natural-killer-cell diversity in mice and humans. Nat Rev Immunol.7:703-14. DOI: https://doi.org/10.1038/nri2154, PMID: 17717540.

38. Freud AG, Caligiuri MA. 2006. Human natural killer cell development. Immunol Rev.214:56-72. DOI: https://doi.org/10.1111/j.1600-065X.2006.00451.x, PMID: 17100876.

39. Cooper MA, Fehniger TA, Caligiuri MA. 2001. The biology of human natural killer-cell subsets. Trends Immunol.22:633-40. DOI: https://doi.org/10.1016/s1471-4906(01)02060-9, PMID: 11698225.

40. Jacobs R, Hintzen G, Kemper A, Beul K, Kempf S, Behrens G, Sykora KW, Schmidt RE. 2001. CD56bright cells differ in their KIR repertoire and cytotoxic features from CD56dim NK cells. Eur J Immunol.31:3121-7. DOI: https://doi.org/10.1002/1521-4141(2001010)31:10<3121::aid-immu3121>3.0.co;2-4, PMID: 11592089.

41. Moretta L. 2010. Dissecting CD56dim human NK cells. Blood.116:3689-91. DOI: https://doi.org/10.1182/blood-2010-09-303057, PMID: 21071612.

42. Tang F, Li J, Qi L, Liu D, Bo Y, Qin S, Miao Y, Yu K, Hou W, Li J, Peng J, Tian Z, Zhu L, Peng H, Wang D, Zhang Z. 2023. A pan-cancer single-cell panorama of human natural killer cells. Cell. DOI: https://doi.org/10.1016/j.cell.2023.07.034, PMID: 37607536.

43. Xia T, Li K, Niu N, Shao Y, Ding D, Thomas DL, Jing H, Fujiwara K, Hu H, Osipov A, Yuan C, Wolfgang CL, Thompson ED, Anders RA, He J, Mou Y, Murphy AG, Zheng L. 2022. Immune cell atlas of cholangiocarcinomas reveals distinct tumor microenvironments and associated prognoses. J Hematol Oncol.15:37. DOI: https://doi.org/10.1186/s13045-022-01253-z, PMID: 35346322.

44. Kim R, An M, Lee H, Mehta A, Heo YJ, Kim KM, Lee SY, Moon J, Kim ST, Min BH, Kim TJ, Rha SY, Kang WK, Park WY, Klempner SJ, Lee J. 2022. Early Tumor-Immune Microenvironmental Remodeling and Response to First-Line Fluoropyrimidine and Platinum Chemotherapy in Advanced Gastric Cancer. Cancer Discov.12:984-1001. DOI: https://doi.org/10.1158/2159-8290.CD-21-0888, PMID: 34933901.

45. Laskowski TJ, Biederstadt A, Rezvani K. 2022. Natural killer cells in antitumour adoptive cell immunotherapy. Nat Rev Cancer.22:557-75. DOI: https://doi.org/10.1038/s41568-022-00491-0, PMID: 35879429.

46. Myers JA, Miller JS. 2021. Exploring the NK cell platform for cancer immunotherapy. Nat Rev Clin Oncol.18:85-100. DOI: https://doi.org/10.1038/s41571-020-0426-7, PMID: 32934330.

47. Thacker G, Henry S, Nandi A, Debnath R, Singh S, Nayak A, Susnik B, Boone MM, Zhang Q, Kesmodel SB, Gumber S, Das GM, Kambayashi T, Dos Santos CO, Chakrabarti R. 2023. Immature natural killer cells promote progression of triple-negative breast cancer. Sci Transl Med.15:eabl4414. DOI: https://doi.org/10.1126/scitranslmed.abl4414, PMID: 36888695.

48. Andre P, Biassoni R, Colonna M, Cosman D, Lanier LL, Long EO, Lopez-Botet M, Moretta A, Moretta L, Parham P, Trowsdale J, Vivier E, Wagtmann N, Wilson MJ. 2001. New nomenclature for MHC receptors. Nat Immunol.2:661. DOI: https://doi.org/10.1038/90589, PMID: 11477395.

49. Faure M, Long EO. 2002. KIR2DL4 (CD158d), an NK cell-activating receptor with inhibitory potential. J Immunol.168:6208-14. DOI: https://doi.org/10.4049/jimmunol.168.12.6208, PMID: 12055234.

50. Kilic N, Dastouri M, Kandemir I, Yilmaz E. 2023. The effects of KIR2DL4 stimulated NK-92 cells on the apoptotic pathways of HER2 + /HER-breast cancer cells. Med Oncol.40:139. DOI:

754 https://doi.org/10.1007/s12032-023-02009-6, PMID: 37027073.
755 51. Yu L, Sun L, Liu X, Wang X, Yan H, Pu Q, Xie Y, Jiang Y, Du J, Yang Z. 2023. The imbalance
756 between NKG2A and NKG2D expression is involved in NK cell immunosuppression and tumor
757 progression of patients with hepatitis B virus-related hepatocellular carcinoma. Hepatol Res.53:417-31.
758 DOI: https://doi.org/10.1111/hepr.13877, PMID: 36628564.
759 52. Hsu YR, Wu GM, Mendiaz EA, Syed R, Wypych J, Toso R, Mann MB, Boone TC, Narhi LO, Lu
760 HS, Langley KE. 1997. The majority of stem cell factor exists as monomer under physiological
761 conditions. Implications for dimerization mediating biological activity. J Biol Chem.272:6406-15. DOI:
762 https://doi.org/10.1074/jbc.272.10.6406, PMID: 9045664.
763 53. Aguilar C, Aguilar C, Lopez-Marure R, Jimenez-Sanchez A, Rocha-Zavaleta L. 2014. Co-
764 stimulation with stem cell factor and erythropoietin enhances migration of c-Kit expressing cervical
765 cancer cells through the sustained activation of ERK1/2. Mol Med Rep.9:1895-902. DOI:
766 https://doi.org/10.3892/mmr.2014.2044, PMID: 24626629.
767 54. Landuzzi L, De Giovanni C, Nicoletti G, Rossi I, Ricci C, Astolfi A, Scopece L, Scotlandi K,
768 Serra M, Bagnara GP, Nanni P, Lollini PL. 2000. The metastatic ability of Ewing's sarcoma cells is
769 modulated by stem cell factor and by its receptor c-kit. Am J Pathol.157:2123-31. DOI:
770 https://doi.org/10.1016/S0002-9440(10)64850-X, PMID: 11106584.
771 55. Yasuda A, Sawai H, Takahashi H, Ochi N, Matsuo Y, Funahashi H, Sato M, Okada Y, Takeyama
772 H, Manabe T. 2007. Stem cell factor/c-kit receptor signaling enhances the proliferation and invasion of
773 colorectal cancer cells through the PI3K/Akt pathway. Dig Dis Sci.52:2292-300. DOI:
774 https://doi.org/10.1007/s10620-007-9759-7, PMID: 17410437.
775 56. Langley KE, Bennett LG, Wypych J, Yancik SA, Liu XD, Westcott KR, Chang DG, Smith KA,
776 Zsebo KM. 1993. Soluble stem cell factor in human serum. Blood.81:656-60. DOI: PMID: 7678995.
777 57. Hao Y, Hao S, Andersen-Nissen E, Mauck WM, 3rd, Zheng S, Butler A, Lee MJ, Wilk AJ, Darby
778 C, Zager M, Hoffman P, Stoeckius M, Papalexi E, Mimitou EP, Jain J, Srivastava A, Stuart T, Fleming
779 LM, Yeung B, Rogers AJ, McElrath JM, Blish CA, Gottardo R, Smibert P, Satija R. 2021. Integrated
780 analysis of multimodal single-cell data. Cell.184:3573-87 e29. DOI:
781 https://doi.org/10.1016/j.cell.2021.04.048, PMID: 34062119.
782 58. Peng Z, Ren Z, Tong Z, Zhu Y, Zhu Y, Hu K. 2023. Interactions between MFAP5 + fibroblasts and
783 tumor-infiltrating myeloid cells shape the malignant microenvironment of colorectal cancer. J Transl
784 Med.21:405. DOI: https://doi.org/10.1186/s12967-023-04281-6, PMID: 37344903.
785 59. Zheng H, Liu H, Ge Y, Wang X. 2021. Integrated single-cell and bulk RNA sequencing analysis
786 identifies a cancer associated fibroblast-related signature for predicting prognosis and therapeutic
787 responses in colorectal cancer. Cancer Cell Int.21:552. DOI: https://doi.org/10.1186/s12935-021-
788 02252-9, PMID: 34670584.
789 60. Hong B, Li Y, Yang R, Dai S, Zhan Y, Zhang WB, Dong R. 2022. Single-cell transcriptional
790 profiling reveals heterogeneity and developmental trajectories of Ewing sarcoma. J Cancer Res Clin
791 Oncol.148:3267-80. DOI: https://doi.org/10.1007/s00432-022-04073-3, PMID: 35713707.
792 61. Qiu X, Hill A, Packer J, Lin D, Ma YA, Trapnell C. 2017. Single-cell mRNA quantification and
793 differential analysis with Census. Nat Methods.14:309-15. DOI: https://doi.org/10.1038/nmeth.4150,
794 PMID: 28114287.
795 62. Goldman MJ, Craft B, Hastie M, Repecka K, McDade F, Kamath A, Banerjee A, Luo Y, Rogers
796 D, Brooks AN, Zhu J, Haussler D. 2020. Visualizing and interpreting cancer genomics data via the
797 Xena platform. Nat Biotechnol.38:675-8. DOI: https://doi.org/10.1038/s41587-020-0546-8, PMID:

32444850.
63. Chen B, Khodadoust MS, Liu CL, Newman AM, Alizadeh AA. 2018. Profiling Tumor Infiltrating Immune Cells with CIBERSORT. Methods Mol Biol.1711:243-59. DOI: https://doi.org/10.1007/978-1-4939-7493-1_12, PMID: 29344893.
64. Aran D, Hu Z, Butte AJ. 2017. xCell: digitally portraying the tissue cellular heterogeneity landscape. Genome Biol.18:220. DOI: https://doi.org/10.1186/s13059-017-1349-1, PMID: 29141660.
65. Racle J, de Jonge K, Baumgaertner P, Speiser DE, Gfeller D. 2017. Simultaneous enumeration of cancer and immune cell types from bulk tumor gene expression data. Elife.6. DOI: https://doi.org/10.7554/eLife.26476, PMID: 29130882.
66. Becht E, Giraldo NA, Lacroix L, Buttard B, Elarouci N, Petitprez F, Selves J, Laurent-Puig P, Sautes-Fridman C, Fridman WH, de Reynies A. 2016. Erratum to: Estimating the population abundance of tissue-infiltrating immune and stromal cell populations using gene expression. Genome Biol.17:249. DOI: https://doi.org/10.1186/s13059-016-1113-y, PMID: 27908289.
67. Yu G, Wang LG, Han Y, He QY. 2012. clusterProfiler: an R package for comparing biological themes among gene clusters. OMICS.16:284-7. DOI: https://doi.org/10.1089/omi.2011.0118, PMID: 22455463.
68. Liberzon A, Birger C, Thorvaldsdottir H, Ghandi M, Mesirov JP, Tamayo P. 2015. The Molecular Signatures Database (MSigDB) hallmark gene set collection. Cell Syst.1:417-25. DOI: https://doi.org/10.1016/j.cels.2015.12.004, PMID: 26771021.

Figure legends

Figure 1. Landscape of tumor immune microenvironment in CCLM revealed by single-cell transcriptomics.

A. Schematic overview of the experimental design and analytical workflow. B. The UMAP plot of all main immune cell types. C. Dot plots showing average expression of known markers in indicated cell clusters. The dot size represents percent of cells expressing the genes in each cluster and the color of dot represents the expression intensity. D. The cell numbers of main immune cells across tissues. E. Proportions of all main immune cells. P values were determined by the paired nonparameter test.

Figure 2. Cellular identification in spatial transcriptomic samples.

A. UMAP visualization of cell clusters in spatial transcriptomic samples. B. Dot plots showing average expression of markers in indicated cell clusters. C. Overview of the spatial transcriptomic sections. H&E staining of spatial transcriptomic sections (upper). Tumor tissue and paratumor tissue identification of each section (middle). Spatial cluster distribution of each section (lower). PC: primary cancer, LM: liver metastasis. D. The signature scores of T cells (upper) and NK cells (lower) in colon cancer and liver metastasis in the spatial transcriptomic sections.

Figure 3. Clinical and biological relationship between NK cells and metastasis of colon cancer revealed by Bulk RNA transcriptomics.

A-D. The relationship of immune cell percentage determined by xCell, EPIC, quanTIseq and MCPCounter between metastasis and non-metastasis tumor in TCGA COAD cohort. E. Volcano plot showing differentially expressed genes between metastasis and non-metastasis colon cancer in TCGA COAD cohort. F. GO and KEGG enriched pathway bar chart of DEGs in metastasis versus non-metastasis colon cancer G. Gene set enrichment analysis (GSEA) of KEGG gene set. H. Natural killer cell mediated cytotoxicity was enriched in the non-metastasis colon cancer.

Figure 4: The landscape of NK cells in the disease progression of CCLM.

A. The UMAP plot of NK cells from CCLM. B. Unsupervised clustering identifies 8 subsets of NK cells. C. Expression of key markers that distinguish resting and activated subsets of NK cells. D. Expression of key resting and activated NK cell markers across all samples. E. The UMAP plot of distribution of resting and activated NK cells from ColonP, ColonT, LiverT and LN. F. Cellular landscape of each sample from the ColonP, ColonT, LiverT and LN. The proportion of NK cells subsets in total immune cells (upper). The proportion of NK cells subsets in total NK cells (lower). G. Number of cells identified from each group (ColonP, ColonT, LiverT and LN) by cell type proportion. H. Proportions of resting (upper) and activated (lower) subsets of NK cells. P values were determined by the paired nonparameter test.

Figure.5 Clinical relationship between NK cells subsets and metastasis of colon cancer revealed by Bulk RNA and spatial transcriptomics.

A-B. The relationship of activated and resting NK cell percentage determined by

863 CIBERSORT and tumor metastasis in TCGA COAD cohort. C-D. K-M survival plots
864 show that high resting NK cell and low activated NK cell predicted poor prognosis in
865 TCGA COAD and GSE29623 cohort. E. The signature scores of resting (upper) and
866 activated NK cells (lower) in colon cancer and liver metastasis in the spatial
867 transcriptomic sections.
868
869 **Figure 6. Characterization and developmental course of differential subsets of**
870 **NK cells in CCLM.**
871 A. The UMAP plot of KIR2DL4+ GPR171+ Activated NK cells, GZMK+ resting NK
872 cells from CCLM. B. Proportions of KIR2DL4+ GPR171+ ActiVated NK cells,
873 GZMK+ resting NK cells in total immune cells. P values were determined by the
874 paired nonparameter test. C. The signature scores of GZMK+ resting NK cells
875 (upper) and KIR2DL4+ GPR171+ Activated NK cells (lower) in colon cancer and
876 liver metastasis in the spatial transcriptomic sections. D. Monocle analysis showing
877 the developmental trajectory of NK cells. Color as in Pseudotime, cell state, subsets of
878 NK cells and sample group. E. Pseudo-temporal change curve of marker genes in
879 each subsets of NK cells. F. The heatmap shows the expression patterns of the top 50
880 significant genes in branched expression analysis modeling, associated GO terms
881 (using DAVID v6.7) are given on the right of the corresponding gene clusters. G-H.
882 The Kaplan–Meier curve shows COAD patients survival with different GZMK+
883 resting NK cells and KIR2DL4+ GPR171+ Activated NK cells infiltration.
884
885 **Figure.7 Colon cancer cells (HCT-116) educated NK cells shift toward tumor**
886 **promoting status depends on cell-to-cell interaction.**
887 A-B. Phenotype switch of NK cells were induced by cell-to-cell interactions with
888 cancer cells. NK cells (NK-92) were cocultured with colon cancer cells (CN),
889 supernatant of cancer cells (SN), or cultured alone (MN), and analyzed by FACS to
890 evaluate the phenotype switch. C. CCK-8 assay showed the NK cell-mediated
891 inductive effect on cell proliferation of colon cancer cell (HCT-116). Colon cancer
892 cells were cultured in the supernatant from co-culture system that NK and cancer cells
893 were cultured in the upper chamber (CNS); cancer cells cultured directly in
894 supernatant that cancer cells were cultured in the upper chamber (CS). D-E. Clone
895 formation assay showed the NK cell–mediated inductive effect on cell proliferation of
896 colon cancer cell (HCT-116). F-H. The NK cell–mediated inductive effect on
897 migration and invasion of colon cancer cell (HCT-116). I. CCK-8 assay showed the
898 NK cell–mediated inductive effect on cell proliferation of colon cancer cell (HCT-
899 116). Colon cancer cells were cultured in the supernatant from different co-culture
900 system in transwell devices. NK cells were cultured with colon cancer cells in contact
901 in the upper chamber of transwell (CNS), with supernatant of cancer cells (SNS), with
902 fresh medium (MNS). J-K. Clone formation assay showed the NK cell–mediated
903 inductive effect on cell proliferation of colon cancer cell (HCT-116). L-N. The NK
904 cell–mediated inductive effect on migration and invasion of colon cancer cell (HCT-
905 116).
906

Figure.8 The resting NK cell promote tumor malignant phenotype via elevating tumor-derived sSCF.

A. luminex liquid suspension chip detection of 48 common chemotactic and inflammatory cytokines in CNS, SNS and MNS group. B-C. Concentration of SCF determined by luminex liquid suspension chip and Elisa in CNS, SNS and MNS group. D-E. CCK-8 assay showed the proliferation of HCT-116 cells was inhibited by imatinib mesylate, evaluated by a CCK-8 assay. Cells were incubated in the supernatant from different co-culture system with DMSO or 2 μM imatinib mesylate. F-I. Clone formation assay showed the proliferation of HCT-116 cells was inhibited by imatinib mesylate. J-M. The NK cell–mediated inductive effect on migration and invasion of HCT-116 was inhibited by imatinib mesylate.

Figure.9. Schematic diagram.

Colon cancer cells (HCT-116 cells) educate NK cells as resting status depends on cell-to-cell interaction. Tumor-educated NK cells subsequent enhances tumor malignancy in a paracrine manner by elevating tumor-derived sSCF.

Figure S1. Cluster characterization of the global landscape of CCLM revealed by single-cell transcriptomics.

A. The UMAP plot of all 12 cell clusters.

B. Dot plots showing average expression of marker genes in indicated cell clusters.

C. The pie chart of the proportion of main immune cells across tissues.

D. The proportion of NK cells in total immune cells of each sample (including PR, PD/SD and untreated patients) from the Liver P, Liver T, Colon P, Colon T.

E. Proportions of NK cells in PR, PD/SD and untreated patients among Liver P, Liver T, Colon P, Colon T groups.

Figure S2. Cellular identification in spatial transcriptomic samples.

A. The UMAP plot of all 11 cell clusters.

B. Dot plots showing average expression of marker genes in indicated cell clusters.

C. Expression of key markers across all samples.

Figure S3. Gene expression features of each sample. The feature plots showed the expression distributions of ALB, CD24, COL1A1, MYH11, CXCL8, CD14, CD79A AND CD3D in each spatial transcriptomic section.

Figure.S4 Clinical relationship between NK cells subsets and colon cancer revealed by TCGA COAD cohort.

A. The relationship of activated and resting NK cell and clinical characteristics of colon cancer in TCGA COAD cohort.

B. The relationship of 22 immune cells percentage determined by CIBERSORT and prognosis of colon cancer in TCGA COAD cohort.

Figure.S5 The proportions of eight clusters of NK cells in Colon P, Colon T, Liver T and LN.

Figure. S6 Schematic overview of the in vitro experimental design.

A. Schematic overview of coculture experiments design.

A. Schematic overview of coculture experiments design in transwells.

Figure.S7 NK cell-mediated tumor promoting effect in colon cancer cells (DLD-1).

A. CCK-8 assay showed the NK cell-mediated inductive effect on cell proliferation of DLD-1 cell among CNS, SNS, MNS groups.

B-C. Clone formation assay showed the NK cell-mediated inductive effect on cell proliferation of DLD-1 cell among CNS, SNS, MNS groups.

D-F. The NK cell–mediated inductive effect on migration and invasion of DLD-1cell among CNS, SNS, MNS groups.

G. CCK-8 assay showed the NK cell–mediated inductive effect on cell proliferation of DLD-1 cell between CNS and CS groups.

H-I. Clone formation assay showed the NK cell–mediated inductive effect on cell proliferation of DLD-1 cell between CNS and CS groups.

J-L. The NK cell–mediated inductive effect on on migration and invasion of DLD-1 cell between CNS and CS groups.

Figure.S8 Relative KITLG expression in different groups.

A. RT-qPCR analysis of KITLG expression in HCT-116 with and without co-cultured with NK cells.

B. RT-qPCR analysis of KITLG expression in HCT-116 and DLD-1 cells.

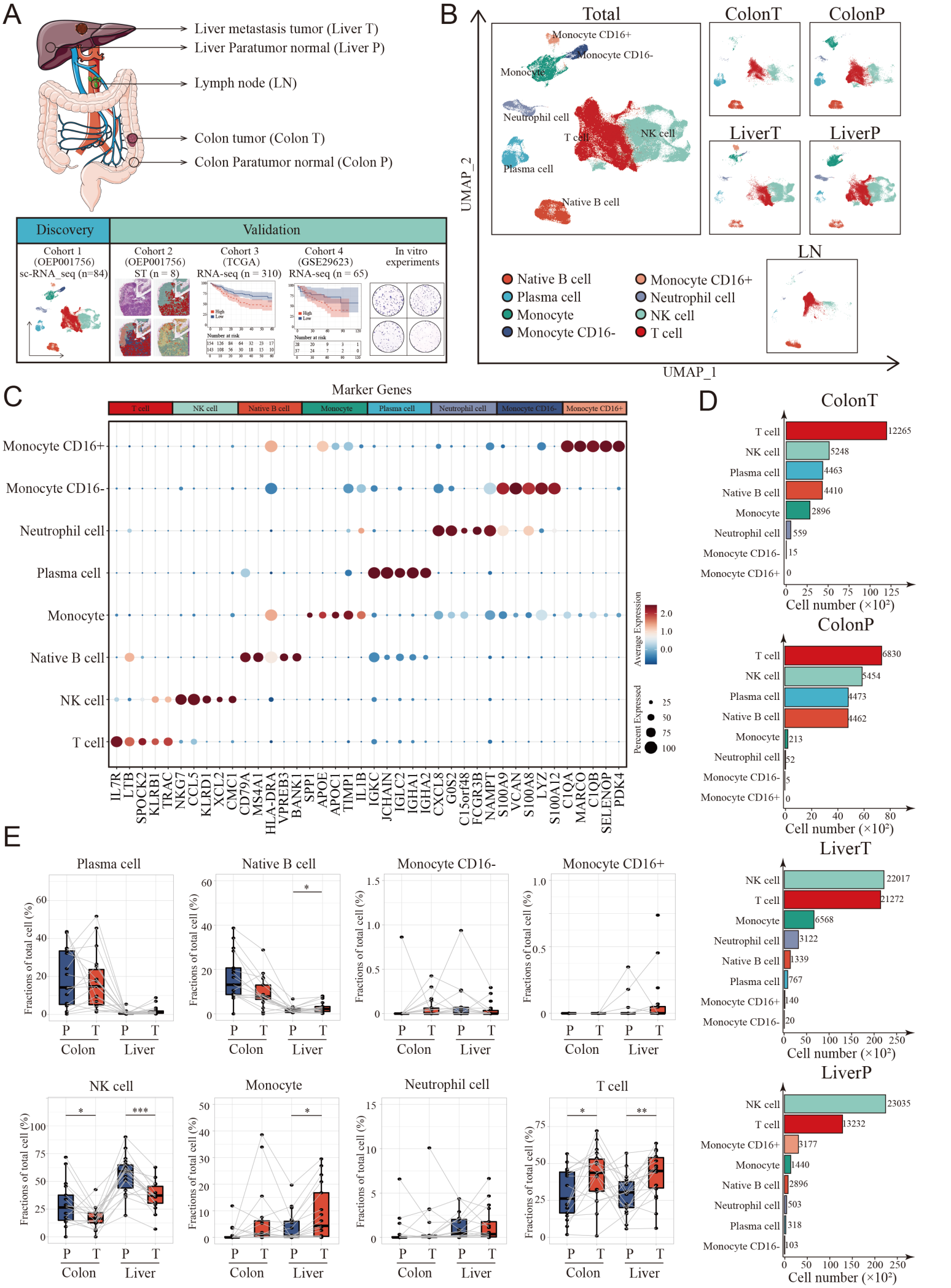
A
Liver metastasis tumor (Liver T)
Liver Paratumor normal (Liver P)
Lymph node (LN)
Colon tumor (Colon T)
Colon Paratumor normal (Colon P)
Discovery
Validation
Cohort 1 (OEP001756) sc-RNA_seq (n=84)
Cohort 2 (OEP001756) ST (n = 8)
Cohort 3 (TCGA) RNA-seq (n = 310)
Cohort 4 (GSE29623) RNA-seq (n = 65)
In vitro experiments
B
Total
ColonT
ColonP
LiverT
LiverP
LN
Monocyte CD16+
Monocyte CD16-
Monocyte
Neutrophil cell
T cell
NK cell
Plasma cell
Native B cell
UMAP_2
UMAP_1
C
Marker Genes
T cell
NK cell
Native B cell
Monocyte
Plasma cell
Neutrophil cell
Monocyte CD16-
Monocyte CD16+
IL7R
LTB
SPOCK2
KLRB1
TRAC
NKG7
CCL5
KLRD1
XCL2
CMC1
CD79A
MS4A1
HLA-DRA
VPREB3
BANK1
SPP1
APOE
APOC1
TIMP1
IL1B
IGKC
JCHAIN
IGLC2
IGHA1
IGHA2
CXCL8
G0S2
C15orf48
FCGR3B
NAMPT
S100A9
VCAN
S100A8
LYZ
S100A12
C1QA
MARCO
C1QB
SELENOP
PDK4
Average Expression
Percent Expressed
D
ColonT
ColonP
LiverT
LiverP
Cell number (×10²)
E
Plasma cell
Native B cell
Monocyte CD16-
Monocyte CD16+
NK cell
Monocyte
Neutrophil cell
T cell
Fractions of total cell (%)
P
T
Colon
Liver

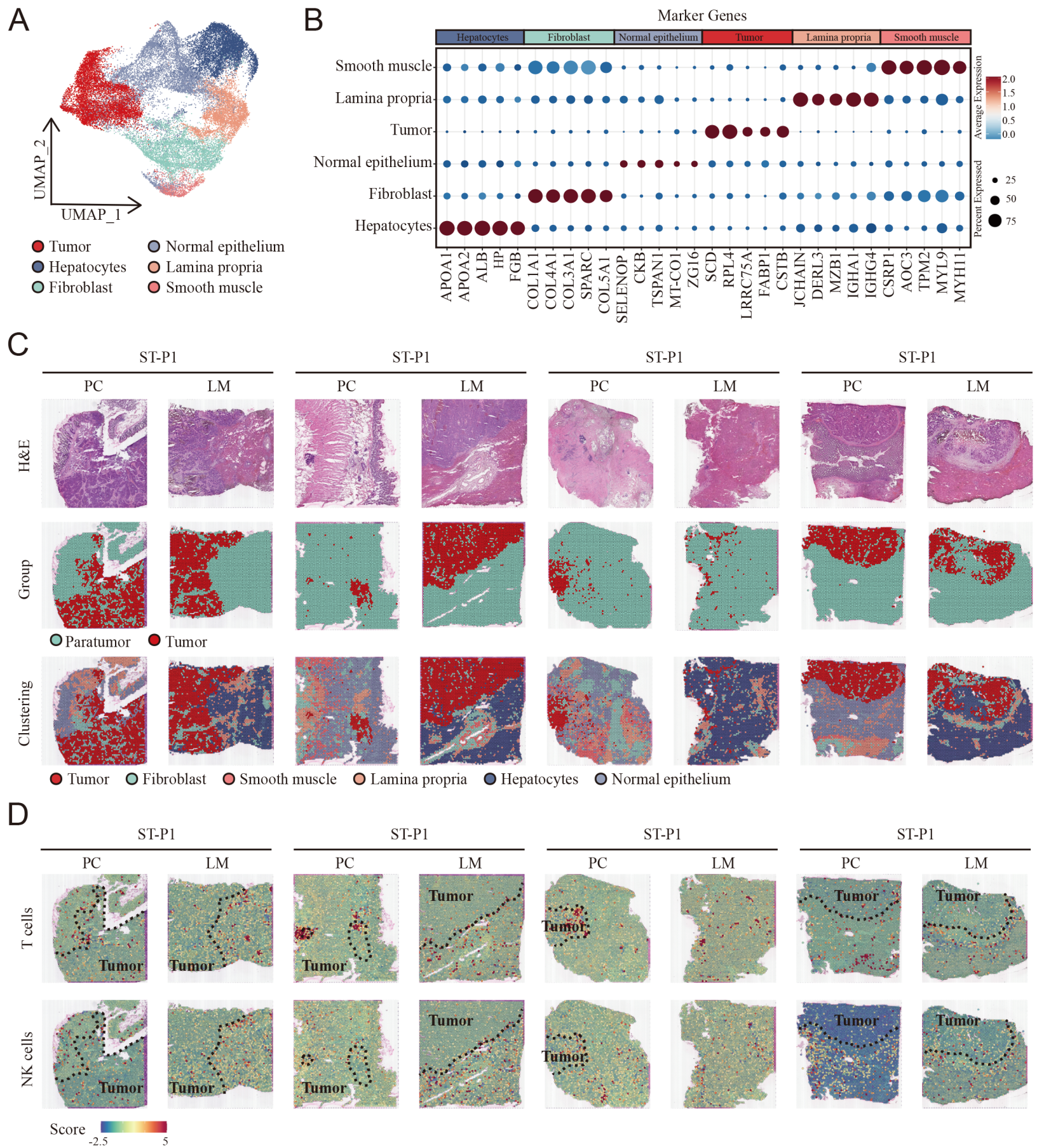
A
UMAP_2
UMAP_1
Tumor
Hepatocytes
Fibroblast
Normal epithelium
Lamina propria
Smooth muscle
B
Marker Genes
Hepatocytes
Fibroblast
Normal epithelium
Tumor
Lamina propria
Smooth muscle
Smooth muscle
Lamina propria
Tumor
Normal epithelium
Fibroblast
Hepatocytes
APOA1
APOA2
ALB
HP
FGB
COL1A1
COL4A1
COL3A1
SPARC
COL5A1
SELENOP
CKB
TSPAN1
MT-CO1
ZG16
SCD
RPL4
LRRC75A
FABP1
CSTB
JCHAIN
DERL3
MZB1
IGHA1
IGHG4
CSRP1
AOC3
TPM2
MYL9
MYH11
Average Expression
2.0
1.5
1.0
0.5
0.0
Percent Expressed
25
50
75
C
ST-P1
PC
LM
H&E
Group
Paratumor
Tumor
Clustering
Tumor
Fibroblast
Smooth muscle
Lamina propria
Hepatocytes
Normal epithelium
D
ST-P1
PC
LM
T cells
NK cells
Tumor
Score
-2.5
5

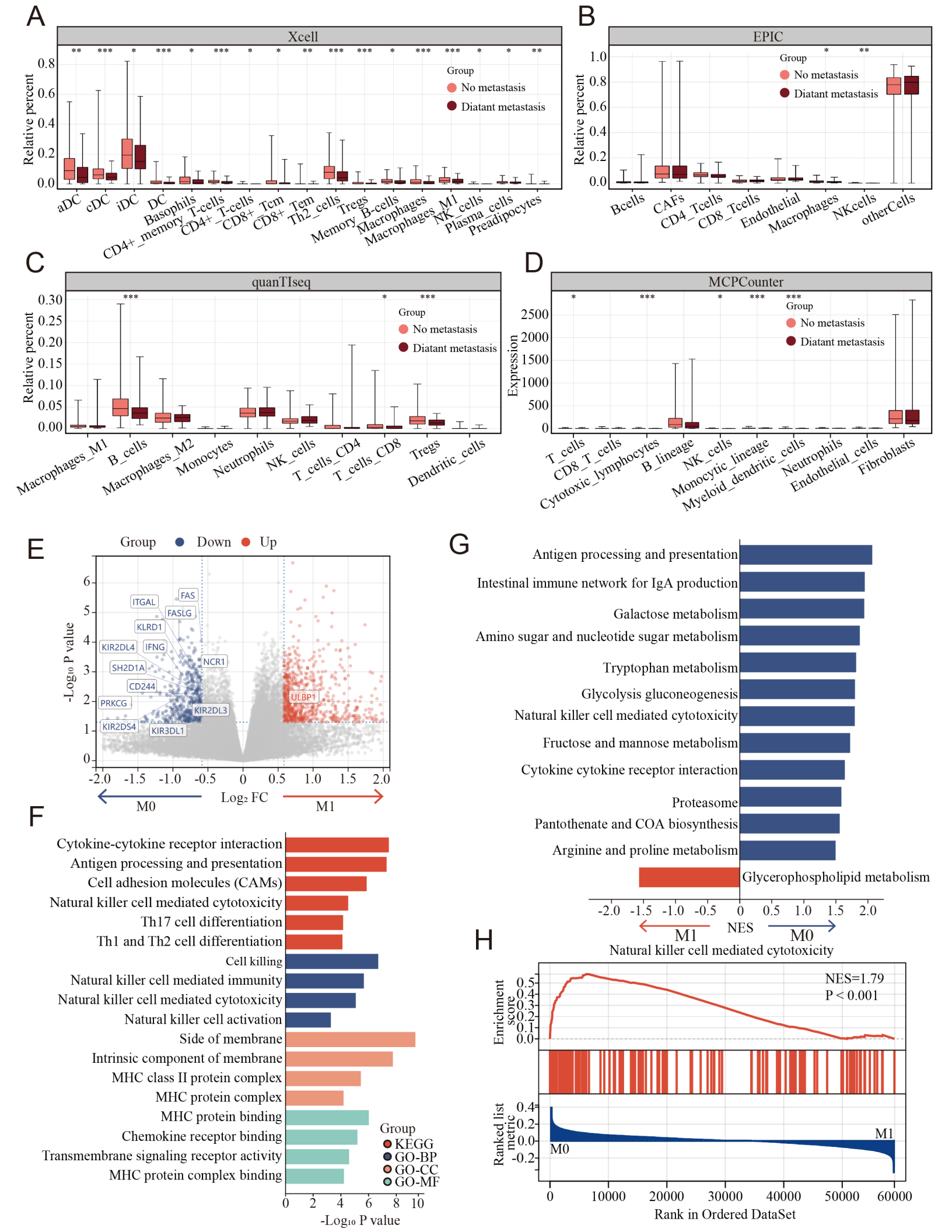
A
Xcell
Relative percent
Group
No metastasis
Diatant metastasis
aDC
cDC
iDC
DC
Basophils
CD4+_memory_T-cells
CD4+_T-cells
CD8+_Tcm
CD8+_Tem
Th2_cells
Tregs
Memory_B-cells
Macrophages
Macrophages_M1
NK_cells
Plasma_cells
Preadipocytes
B
EPIC
Relative percent
Group
No metastasis
Diatant metastasis
Bcells
CAFs
CD4_Tcells
CD8_Tcells
Endothelial
Macrophages
NKcells
otherCells
C
quanTIseq
Relative percent
Group
No metastasis
Diatant metastasis
Macrophages_M1
B_cells
Macrophages_M2
Monocytes
Neutrophils
NK_cells
T_cells_CD4
T_cells_CD8
Tregs
Dendritic_cells
D
MCPCounter
Expression
Group
No metastasis
Diatant metastasis
T_cells
CD8_T_cells
Cytotoxic_lymphocytes
B_lineage
NK_cells
Monocytic_lineage
Myeloid_dendritic_cells
Neutrophils
Endothelial_cells
Fibroblasts
E
Group
Down
Up
-Log10 P value
ITGAL
FAS
FASLG
KLRD1
KIR2DL4
IFNG
NCR1
SH2D1A
CD244
PRKCG
KIR2DL3
KIR2DS4
KIR3DL1
ULBP1
Log2 FC
M0
M1
F
Cytokine-cytokine receptor interaction
Antigen processing and presentation
Cell adhesion molecules (CAMs)
Natural killer cell mediated cytotoxicity
Th17 cell differentiation
Th1 and Th2 cell differentiation
Cell killing
Natural killer cell mediated immunity
Natural killer cell mediated cytotoxicity
Natural killer cell activation
Side of membrane
Intrinsic component of membrane
MHC class II protein complex
MHC protein complex
MHC protein binding
Chemokine receptor binding
Transmembrane signaling receptor activity
MHC protein complex binding
Group
KEGG
GO-BP
GO-CC
GO-MF
-Log10 P value
G
Antigen processing and presentation
Intestinal immune network for IgA production
Galactose metabolism
Amino sugar and nucleotide sugar metabolism
Tryptophan metabolism
Glycolysis gluconeogenesis
Natural killer cell mediated cytotoxicity
Fructose and mannose metabolism
Cytokine cytokine receptor interaction
Proteasome
Pantothenate and COA biosynthesis
Arginine and proline metabolism
Glycerophospholipid metabolism
NES
M1
M0
H
Natural killer cell mediated cytotoxicity
NES=1.79
P < 0.001
Enrichment score
Ranked list metric
M0
M1
Rank in Ordered DataSet

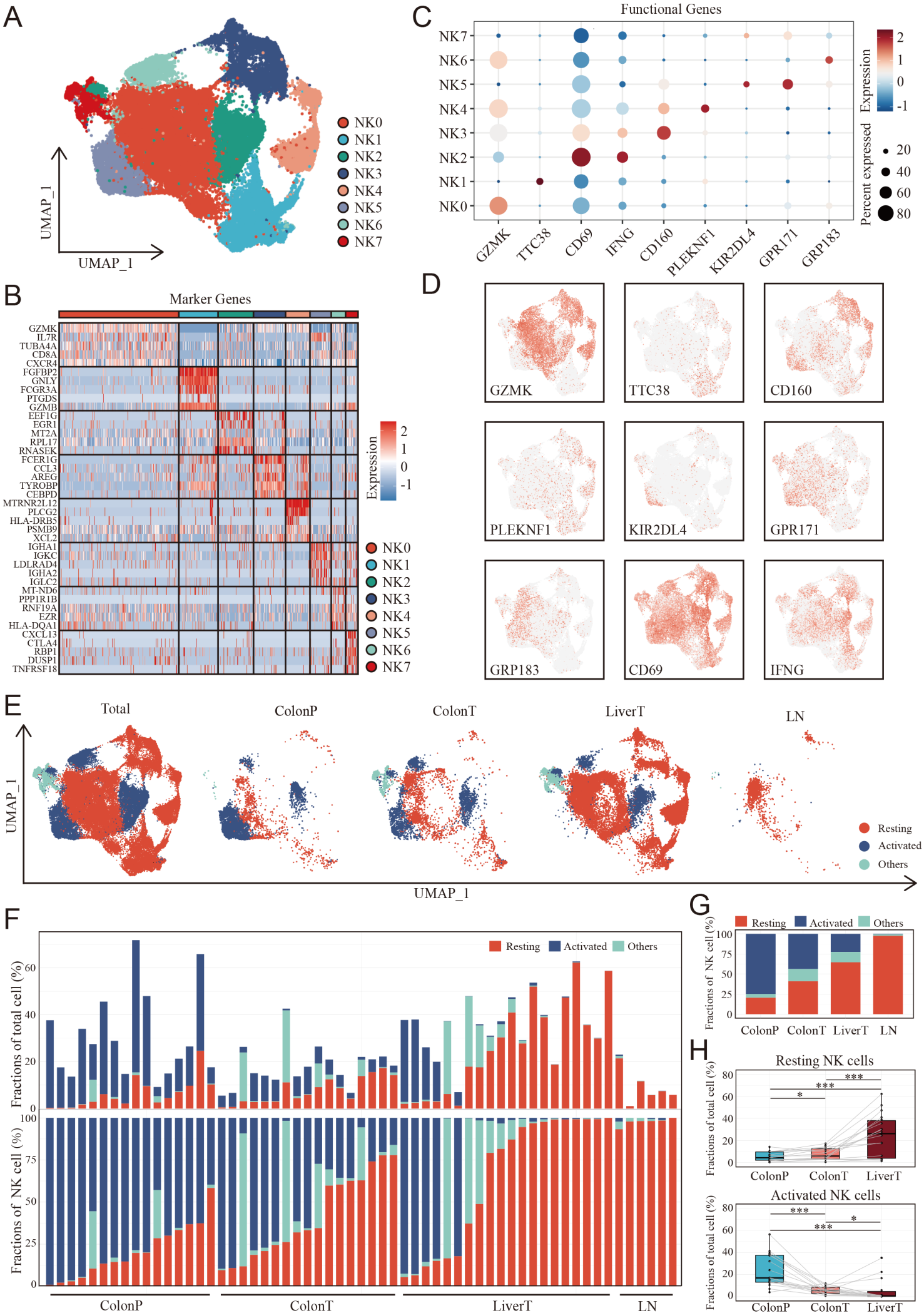
A
UMAP_1
UMAP_1
NK0
NK1
NK2
NK3
NK4
NK5
NK6
NK7
C
Functional Genes
NK7
NK6
NK5
NK4
NK3
NK2
NK1
NK0
GZMK
TTC38
CD69
IFNG
CD160
PLEKNF1
KIR2DL4
GPR171
GRP183
Expression
Percent expressed
B
Marker Genes
GZMK
IL7R
TUBA4A
CD8A
CXCR4
FGFBP2
GNLY
FCGR3A
PTGDS
GZMB
EEF1G
EGR1
MT2A
RPL17
RNASEK
FCER1G
CCL3
AREG
TYROBP
CEBPD
MTRNR2L12
PLCG2
HLA-DRB5
PSMB9
XCL2
IGHA1
IGKC
LDLRAD4
IGHA2
IGLC2
MT-ND6
PPP1R1B
RNF19A
EZR
HLA-DQA1
CXCL13
CTLA4
RBP1
DUSP1
TNFRSF18
Expression
D
GZMK
TTC38
CD160
PLEKNF1
KIR2DL4
GPR171
GRP183
CD69
IFNG
E
Total
ColonP
ColonT
LiverT
LN
UMAP_1
UMAP_1
Resting
Activated
Others
F
Resting
Activated
Others
Fractions of total cell (%)
Fractions of NK cell (%)
ColonP
ColonT
LiverT
LN
G
Resting
Activated
Others
Fractions of NK cell (%)
ColonP
ColonT
LiverT
LN
H
Resting NK cells
Fractions of total cell (%)
ColonP
ColonT
LiverT
Activated NK cells
Fractions of total cell (%)
ColonP
ColonT
LiverT

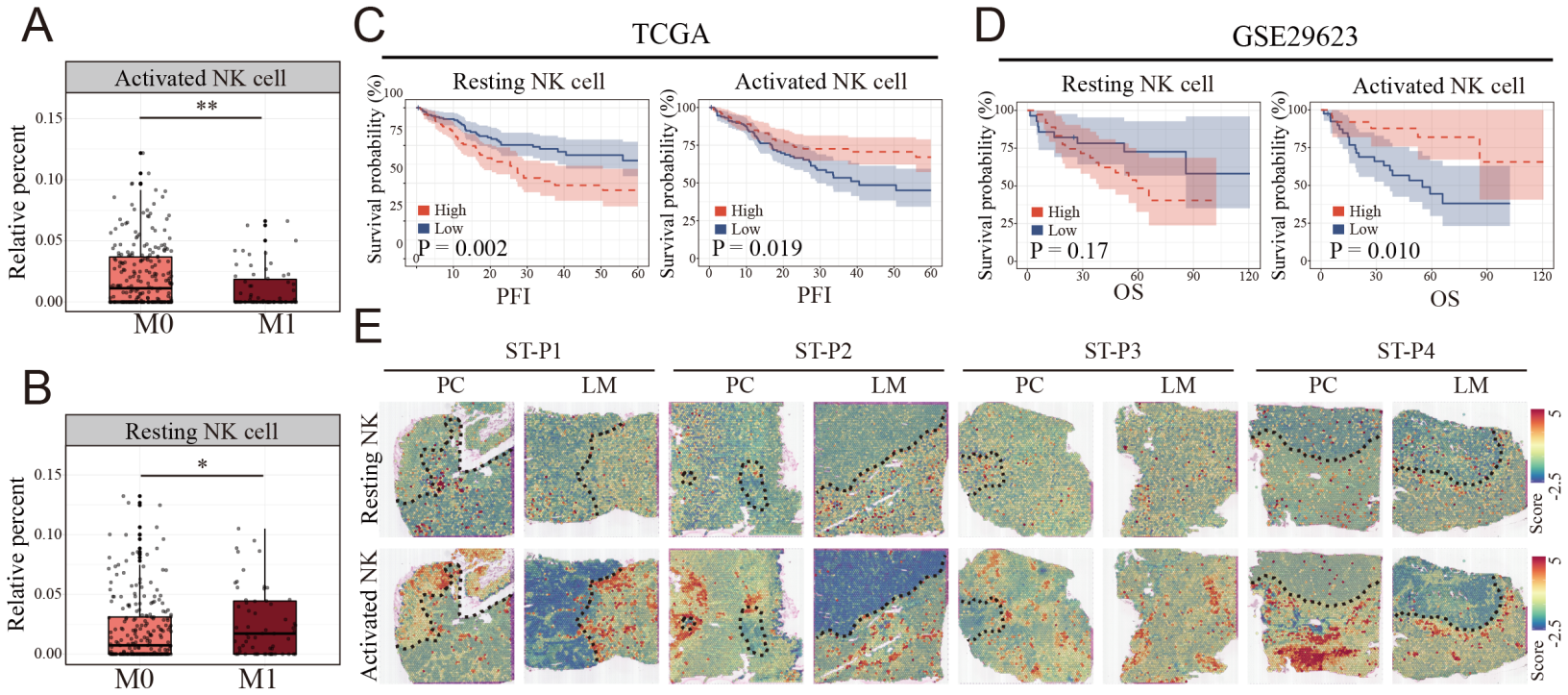
A
Activated NK cell
**
Relative percent
0.15
0.10
0.05
0.00
M0
M1
B
Resting NK cell
*
Relative percent
0.15
0.10
0.05
0.00
M0
M1
C
TCGA
Resting NK cell
Activated NK cell
Survival probability (%)
High
Low
P = 0.002
P = 0.019
PFI
D
GSE29623
Resting NK cell
Activated NK cell
Survival probability (%)
High
Low
P = 0.17
P = 0.010
OS
E
ST-P1
ST-P2
ST-P3
ST-P4
PC
LM
Resting NK
Activated NK
Score
5
-2.5

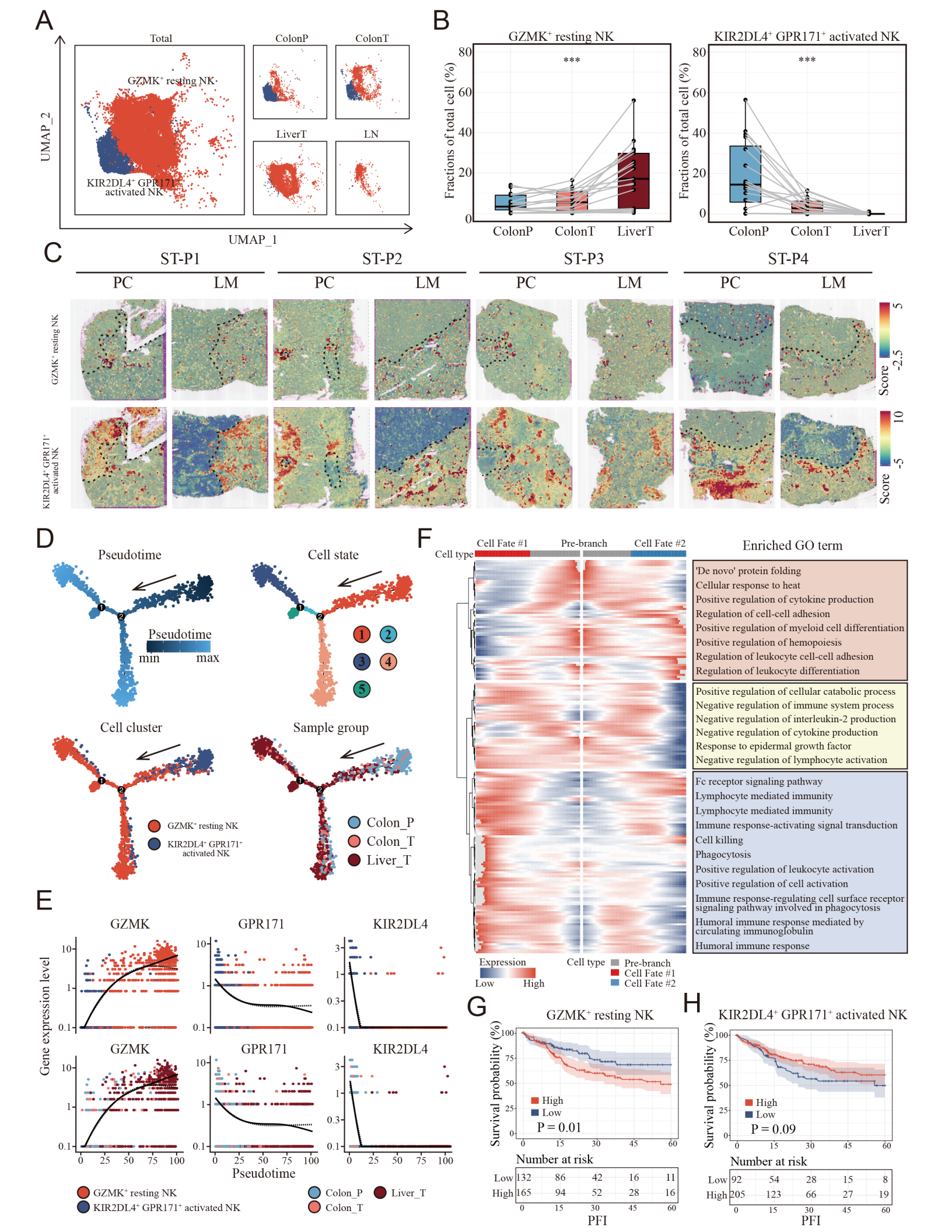
A
Total
ColonP
ColonT
LiverT
LN
GZMK+ resting NK
KIR2DL4+ GPR171+ activated NK
UMAP_2
UMAP_1
B
GZMK+ resting NK
KIR2DL4+ GPR171+ activated NK
Fractions of total cell (%)
***
ColonP
ColonT
LiverT
C
ST-P1
ST-P2
ST-P3
ST-P4
PC
LM
GZMK+ resting NK
KIR2DL4+ GPR171+ activated NK
Score
D
Pseudotime
Cell state
Cell cluster
Sample group
min
max
GZMK+ resting NK
KIR2DL4+ GPR171+ activated NK
Colon_P
Colon_T
Liver_T
E
GZMK
GPR171
KIR2DL4
Gene expression level
Pseudotime
GZMK+ resting NK
KIR2DL4+ GPR171+ activated NK
Colon_P
Colon_T
Liver_T
F
Cell Fate #1
Pre-branch
Cell Fate #2
Cell type
Enriched GO term
'De novo' protein folding
Cellular response to heat
Positive regulation of cytokine production
Regulation of cell-cell adhesion
Positive regulation of myeloid cell differentiation
Positive regulation of hemopoiesis
Regulation of leukocyte cell-cell adhesion
Regulation of leukocyte differentiation
Positive regulation of cellular catabolic process
Negative regulation of immune system process
Negative regulation of interleukin-2 production
Negative regulation of cytokine production
Response to epidermal growth factor
Negative regulation of lymphocyte activation
Fc receptor signaling pathway
Lymphocyte mediated immunity
Lymphocyte mediated immunity
Immune response-activating signal transduction
Cell killing
Phagocytosis
Positive regulation of leukocyte activation
Positive regulation of cell activation
Immune response-regulating cell surface receptor signaling pathway involved in phagocytosis
Humoral immune response mediated by circulating immunoglobulin
Humoral immune response
Expression
Low
High
Cell type
Pre-branch
Cell Fate #1
Cell Fate #2
G
GZMK+ resting NK
Survival probability (%)
High
Low
P = 0.01
Number at risk
Low 132 86 42 16 11
High 165 94 52 28 16
PFI
H
KIR2DL4+ GPR171+ activated NK
Survival probability (%)
High
Low
P = 0.09
Number at risk
Low 92 54 28 15 8
High 205 123 66 27 19
PFI

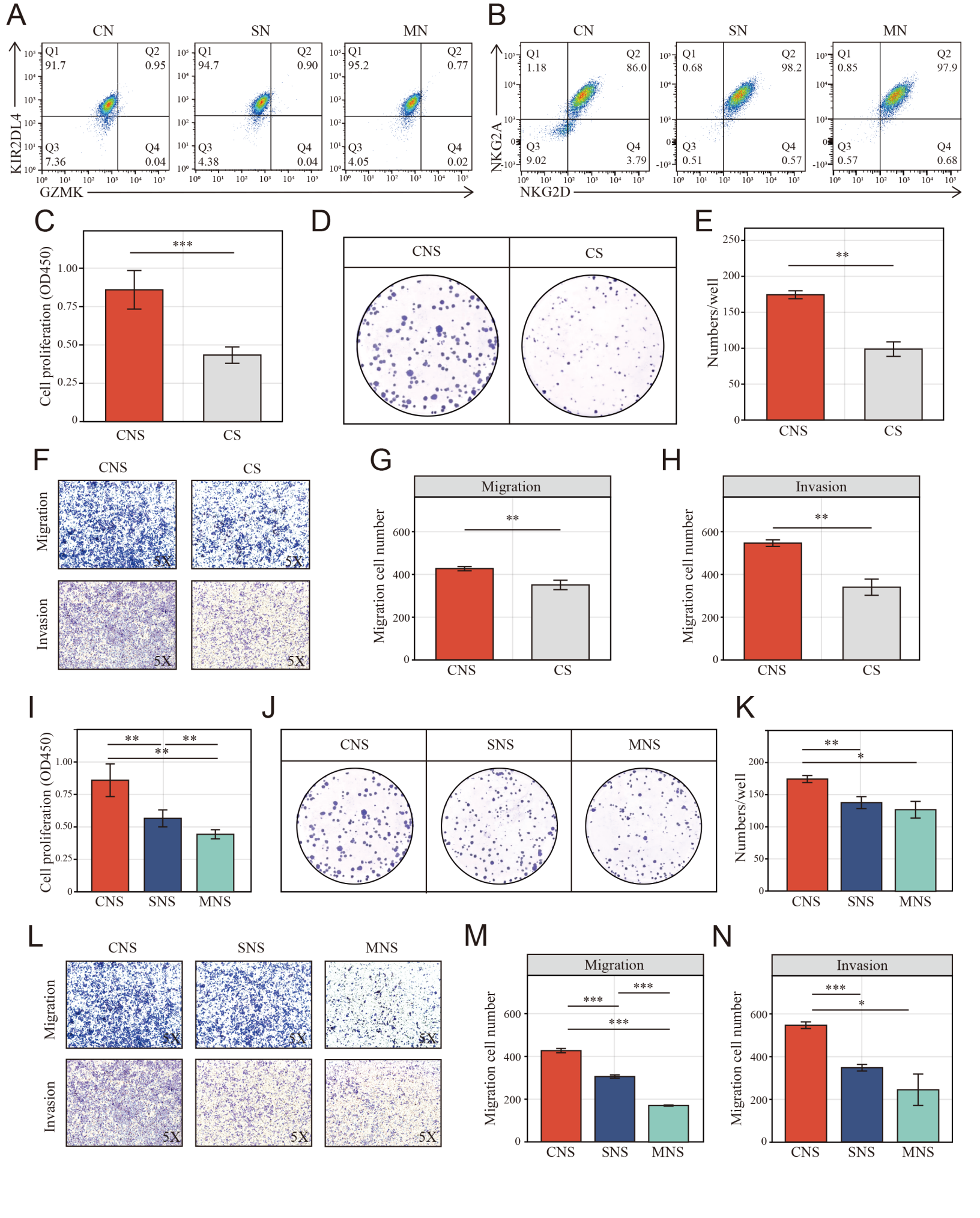
A
CN
SN
MN
KIR2DL4
GZMK
Q1 91.7
Q2 0.95
Q3 7.36
Q4 0.04
Q1 94.7
Q2 0.90
Q3 4.38
Q4 0.04
Q1 95.2
Q2 0.77
Q3 4.05
Q4 0.02
B
NKG2A
NKG2D
Q1 1.18
Q2 86.0
Q3 9.02
Q4 3.79
Q1 0.68
Q2 98.2
Q3 0.51
Q4 0.57
Q1 0.85
Q2 97.9
Q3 0.57
Q4 0.68
C
Cell proliferation (OD450)
***
CNS
CS
D
CNS
CS
E
Numbers/well
**
CNS
CS
F
CNS
CS
Migration
Invasion
5X
G
Migration
Migration cell number
**
CNS
CS
H
Invasion
Migration cell number
**
CNS
CS
I
Cell proliferation (OD450)
**
**
**
CNS
SNS
MNS
J
CNS
SNS
MNS
K
Numbers/well
**
*
CNS
SNS
MNS
L
CNS
SNS
MNS
Migration
Invasion
5X
M
Migration
Migration cell number
***
***
***
CNS
SNS
MNS
N
Invasion
Migration cell number
***
*
CNS
SNS
MNS

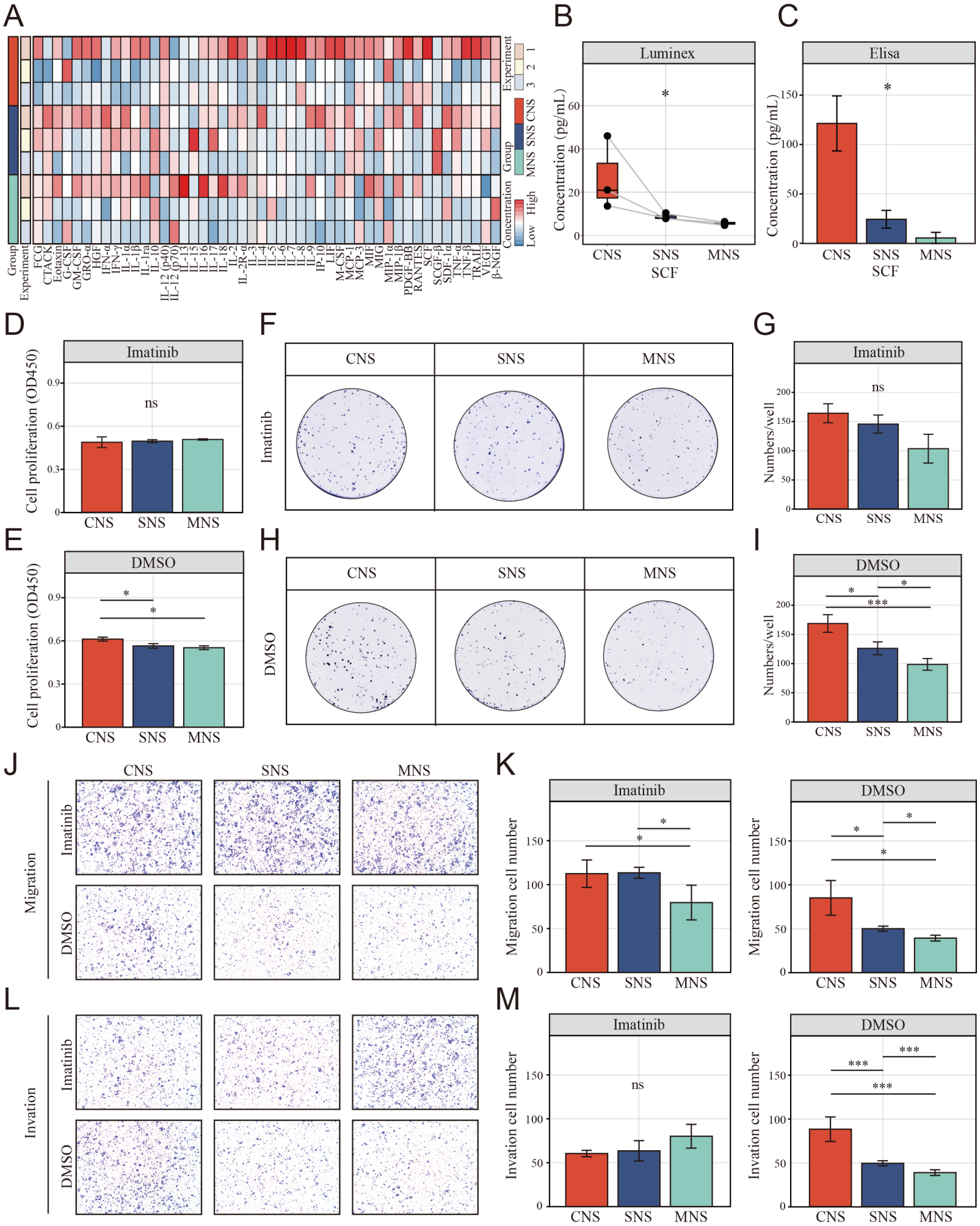
A
Group
Experiment
FCG
CTACK
Eotaxin
G-CSF
GM-CSF
GRO-α
HGF
IFN-α
IFN-γ
IL-1α
IL-1β
IL-1ra
IL-10
IL-12 (p40)
IL-12 (p70)
IL-13
IL-15
IL-16
IL-17
IL-18
IL-2
IL-2R-α
IL-3
IL-4
IL-5
IL-6
IL-7
IL-8
IL-9
IP-10
LIF
M-CSF
MCP-1
MCP-3
MIF
MIG
MIP-1α
MIP-1β
PDGF-BB
RANTES
SCF
SCGF-β
SDF-1α
TNF-α
TNF-β
TRAIL
VEGF
β-NGF
Experiment
1
2
3
Group
CNS
SNS
MNS
Concentration
High
Low
B
Luminex
Concentration (pg/mL)
CNS
SNS
MNS
SCF
C
Elisa
Concentration (pg/mL)
CNS
SNS
MNS
SCF
D
Imatinib
Cell proliferation (OD450)
ns
CNS
SNS
MNS
E
DMSO
Cell proliferation (OD450)
CNS
SNS
MNS
F
CNS
SNS
MNS
Imatinib
G
Imatinib
Numbers/well
ns
CNS
SNS
MNS
H
CNS
SNS
MNS
DMSO
I
DMSO
Numbers/well
CNS
SNS
MNS
J
CNS
SNS
MNS
Migration
Imatinib
DMSO
K
Imatinib
Migration cell number
CNS
SNS
MNS
DMSO
Migration cell number
CNS
SNS
MNS
L
Invation
Imatinib
DMSO
M
Imatinib
Invation cell number
ns
CNS
SNS
MNS
DMSO
Invation cell number
CNS
SNS
MNS

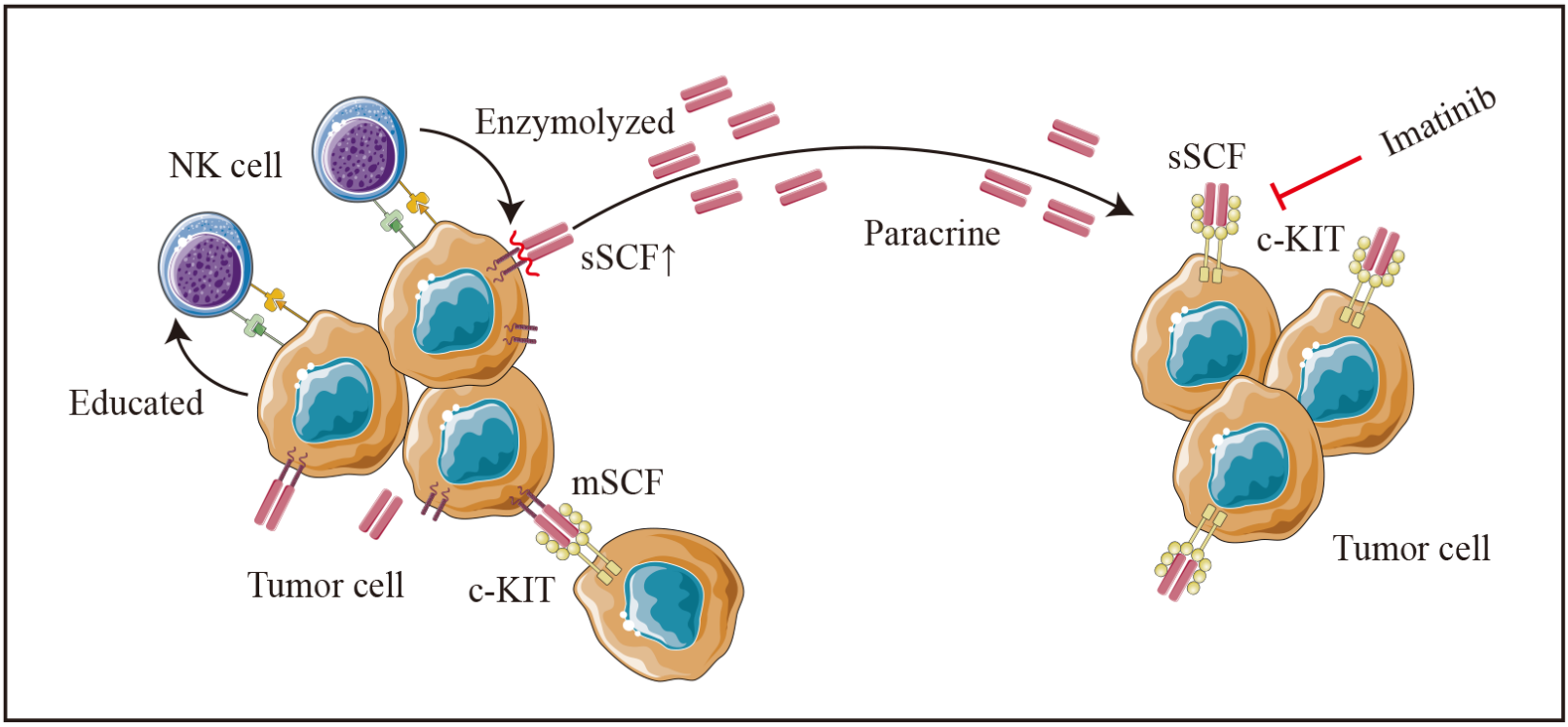
NK cell
Enzymolyzed
sSCF↑
Paracrine
sSCF
Imatinib
c-KIT
Educated
mSCF
Tumor cell
c-KIT
Tumor cell

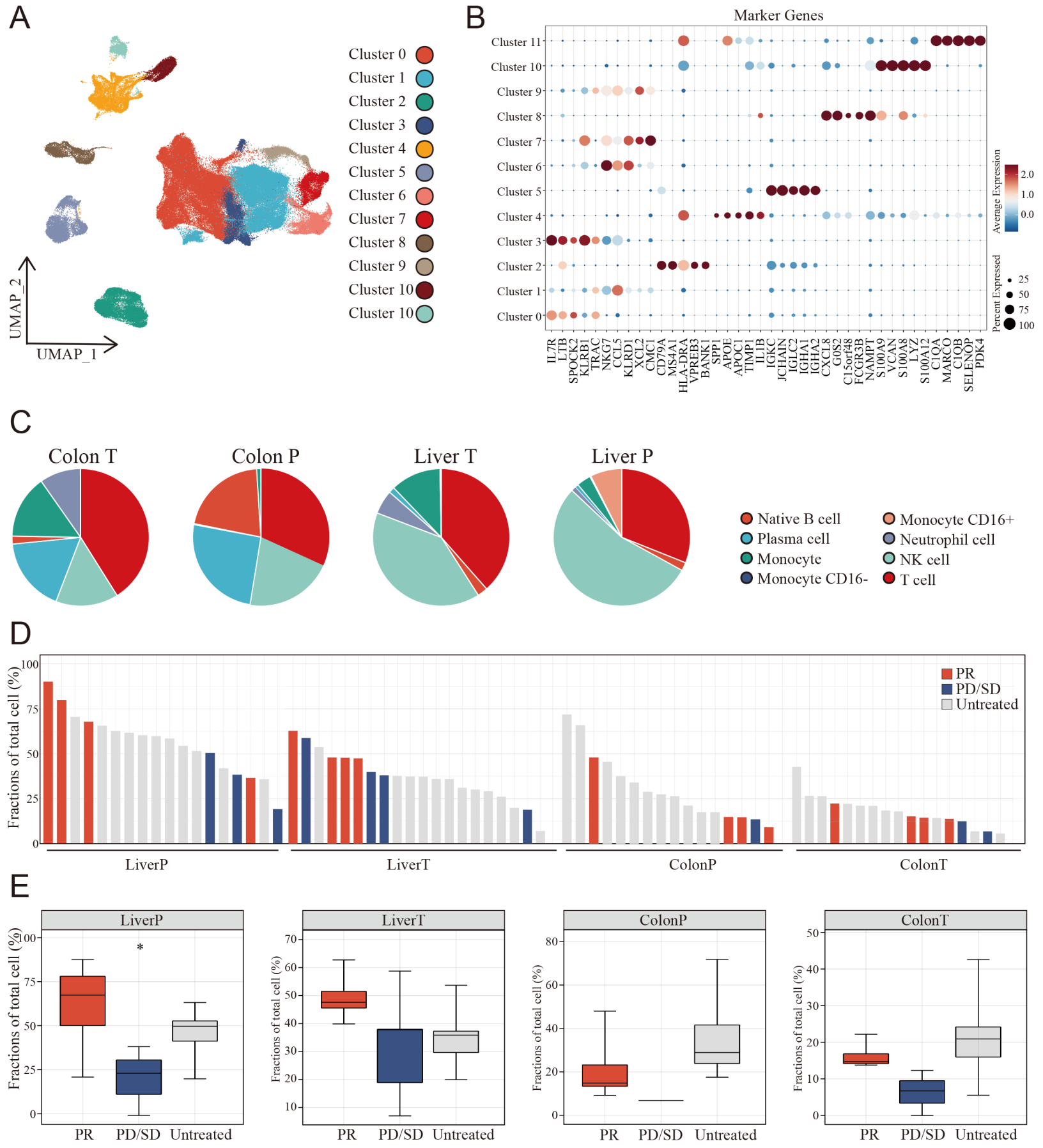
A
Cluster 0
Cluster 1
Cluster 2
Cluster 3
Cluster 4
Cluster 5
Cluster 6
Cluster 7
Cluster 8
Cluster 9
Cluster 10
Cluster 10
UMAP_2
UMAP_1
B
Marker Genes
Cluster 11
Cluster 10
Cluster 9
Cluster 8
Cluster 7
Cluster 6
Cluster 5
Cluster 4
Cluster 3
Cluster 2
Cluster 1
Cluster 0
IL7R
LTB
SPOCK2
KLRB1
TRAC
NKG7
CCL5
KLRD1
XCL2
CMC1
CD79A
MS4A1
HLA-DRA
VPREB3
BANK1
SPP1
APOE
APOC1
TIMP1
IL1B
IGKC
JCHAIN
IGLC2
IGHA1
IGHA2
CXCL8
G0S2
C15orf48
FCGR3B
NAMPT
S100A9
VCAN
S100A8
LYZ
S100A12
C1QA
MARCO
C1QB
SELENOP
PDK4
Average Expression
2.0
1.0
0.0
Percent Expressed
25
50
75
100
C
Colon T
Colon P
Liver T
Liver P
Native B cell
Plasma cell
Monocyte
Monocyte CD16-
Monocyte CD16+
Neutrophil cell
NK cell
T cell
D
Fractions of total cell (%)
100
75
50
25
0
PR
PD/SD
Untreated
LiverP
LiverT
ColonP
ColonT
E
LiverP
LiverT
ColonP
ColonT
Fractions of total cell (%)
PR
PD/SD
Untreated

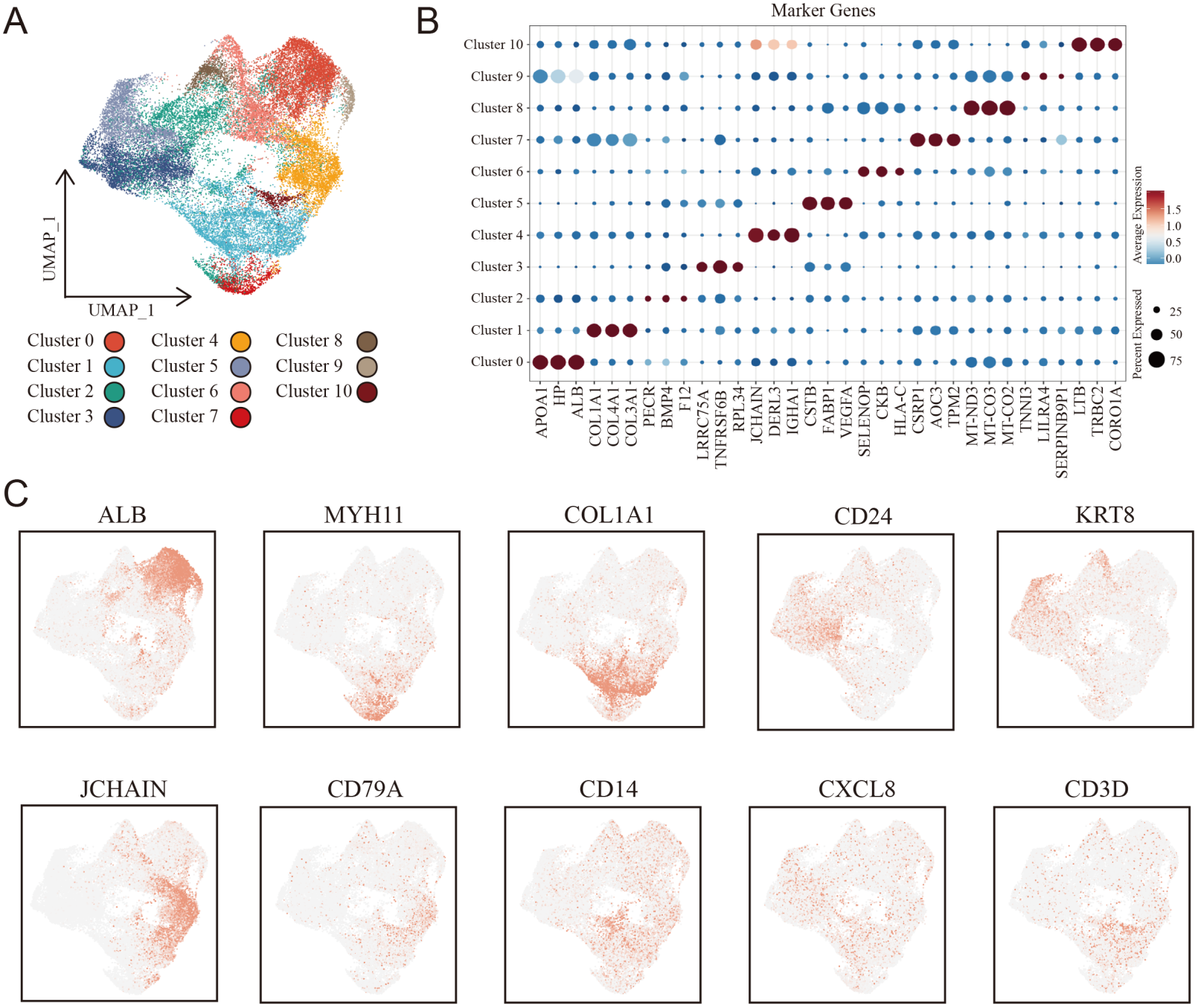
A
UMAP_1
UMAP_1
Cluster 0
Cluster 1
Cluster 2
Cluster 3
Cluster 4
Cluster 5
Cluster 6
Cluster 7
Cluster 8
Cluster 9
Cluster 10
B
Marker Genes
Cluster 10
Cluster 9
Cluster 8
Cluster 7
Cluster 6
Cluster 5
Cluster 4
Cluster 3
Cluster 2
Cluster 1
Cluster 0
APOA1
HP
ALB
COL1A1
COL4A1
COL3A1
PECR
BMP4
F12
LRRC75A
TNFRSF6B
RPL34
JCHAIN
DERL3
IGHA1
CSTB
FABP1
VEGFA
SELENOP
CKB
HLA-C
CSRP1
AOC3
TPM2
MT-ND3
MT-CO3
MT-CO2
TNNI3
LILRA4
SERPINB9P1
LTB
TRBC2
CORO1A
Average Expression
1.5
1.0
0.5
0.0
Percent Expressed
25
50
75
C
ALB
MYH11
COL1A1
CD24
KRT8
JCHAIN
CD79A
CD14
CXCL8
CD3D

ST-P1
ST-P1
ST-P1
ST-P1
PC
LM
PC
LM
PC
LM
PC
LM
ALB
CD24
COL1A1
MYH11
CXCL8
CD14
CD79A
CD3D
Score
Low
High

A

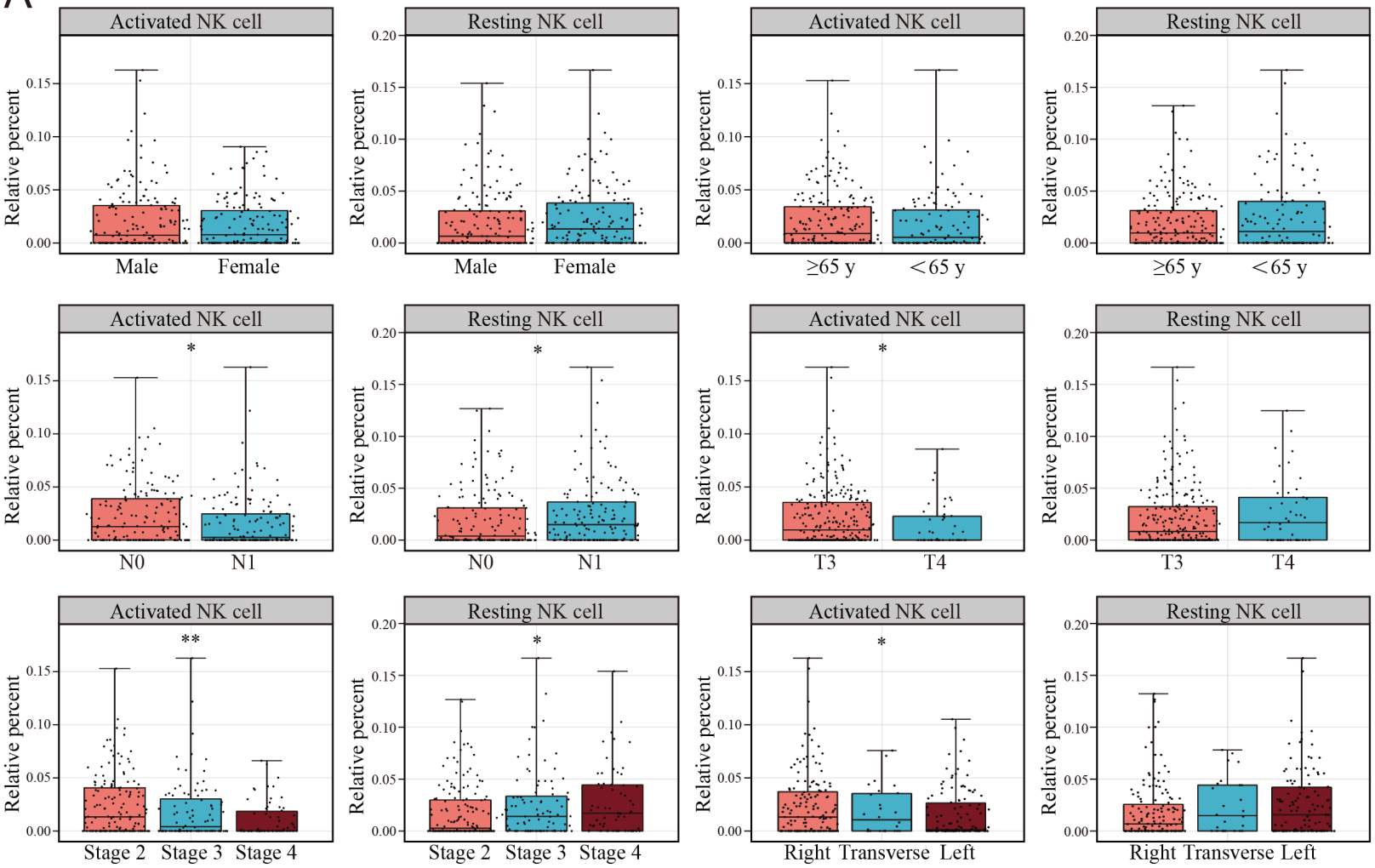

B

Cell type	Cox p. value	HR (95% CI for HR)
Neutrophils (*)	0.03	1.58 (1.05-2.38)
NK.cells. resting (*)	0.017	1.94 (1.27-2.94)
NK.cells. activated (*)	0.04	0.65 (0.43-0.98)
Macrophages.M1 (*)	0.02	0.62 (0.41-0.94)
Dendritic.cells.resting	0.07	0.68 (0.45-1.03)
Mast.cells.resting	0.55	0.86 (0.53-1.40)
Mast.cells.activated	0.13	1.38 (0.91-2.08)
B.cells.memory	0.08	1.43 (0.95-2.16)
T.cells.regulatory.Tregs	0.85	0.96 (0.64-1.45)
Monocytes	0.28	1.25 (0.83-1.89)
T.cells.CD4.memory.resting	0.44	0.85 (0.57-1.28)
T.cells.CD8	0.11	0.72 (0.47-1.08)
Macrophages.M0	0.54	1.14 (0.76-1.71)
Plasma.cells	0.91	1.02 (0.68-1.54)
T.cells.CD4.memory.activated	0.09	0.69 (0.45-1.07)
T.cells.follicular.helper	0.55	1.13 (0.75-1.70)
T.cells.gamma.delta	0.8	0.84 (0.21-3.39)
Eosinophils	0.93	0.98 (0.60-1.59)
Macrophages.M2	0.78	1.06 (0.70-1.59)
T.cells.CD4.naive	0.63	1.21 (0.56-2.62)
B.cells.naive	0.35	1.22 (0.81-1.83)
Dendritic.cells.activated	0.23	1.29 (0.85-1.95)

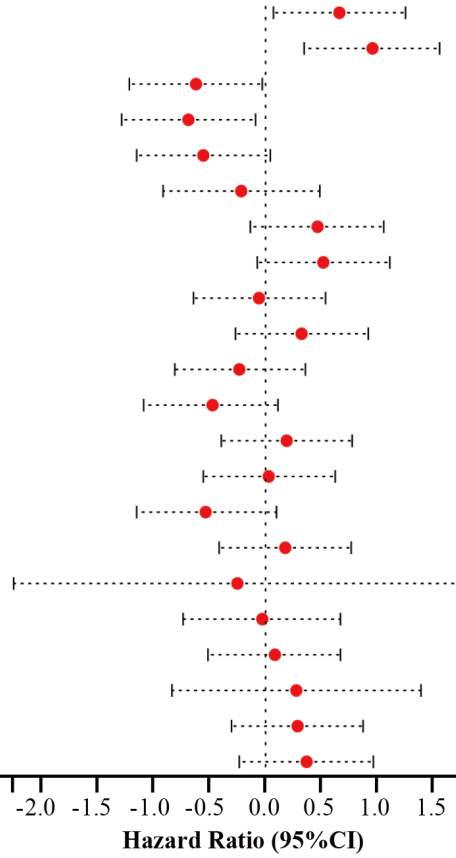

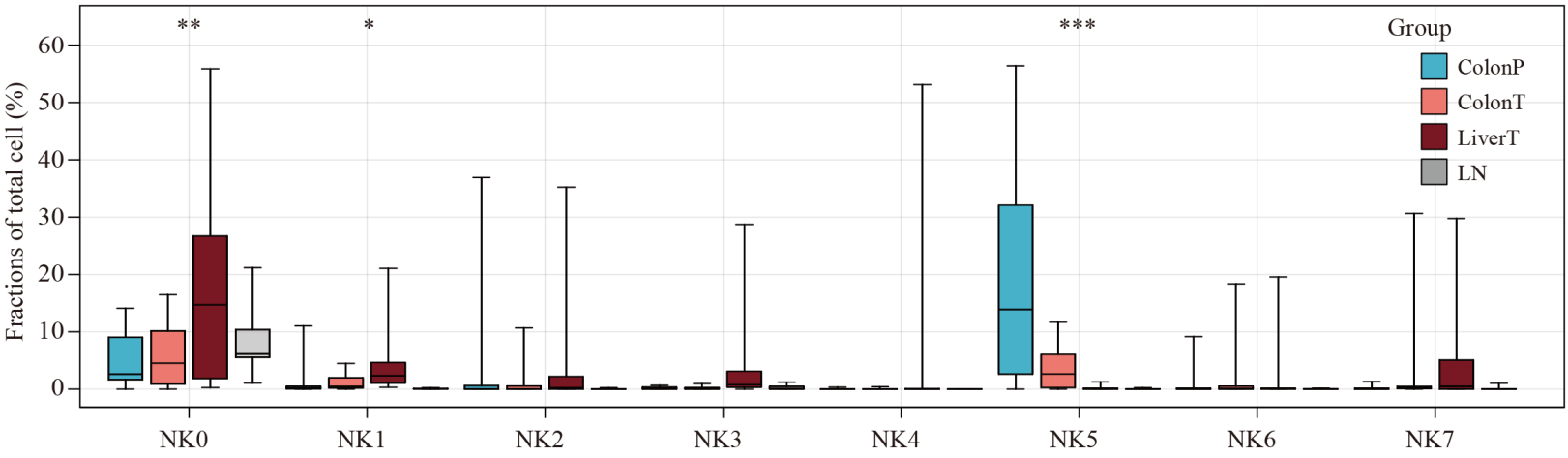
Fractions of total cell (%)
60
50
40
30
20
10
0
**
*
***
Group
ColonP
ColonT
LiverT
LN
NK0
NK1
NK2
NK3
NK4
NK5
NK6
NK7

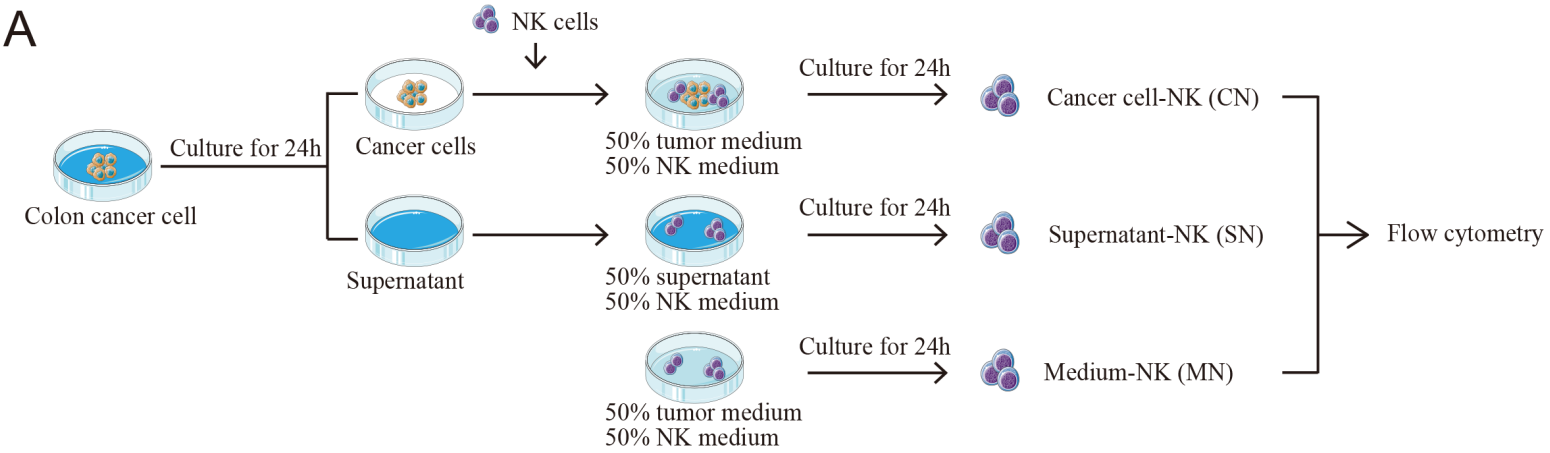
A
NK cells
Culture for 24h
Cancer cell-NK (CN)
Cancer cells
50% tumor medium
50% NK medium
Culture for 24h
Colon cancer cell
Culture for 24h
Supernatant-NK (SN)
Flow cytometry
Supernatant
50% supernatant
50% NK medium
Culture for 24h
Medium-NK (MN)
50% tumor medium
50% NK medium

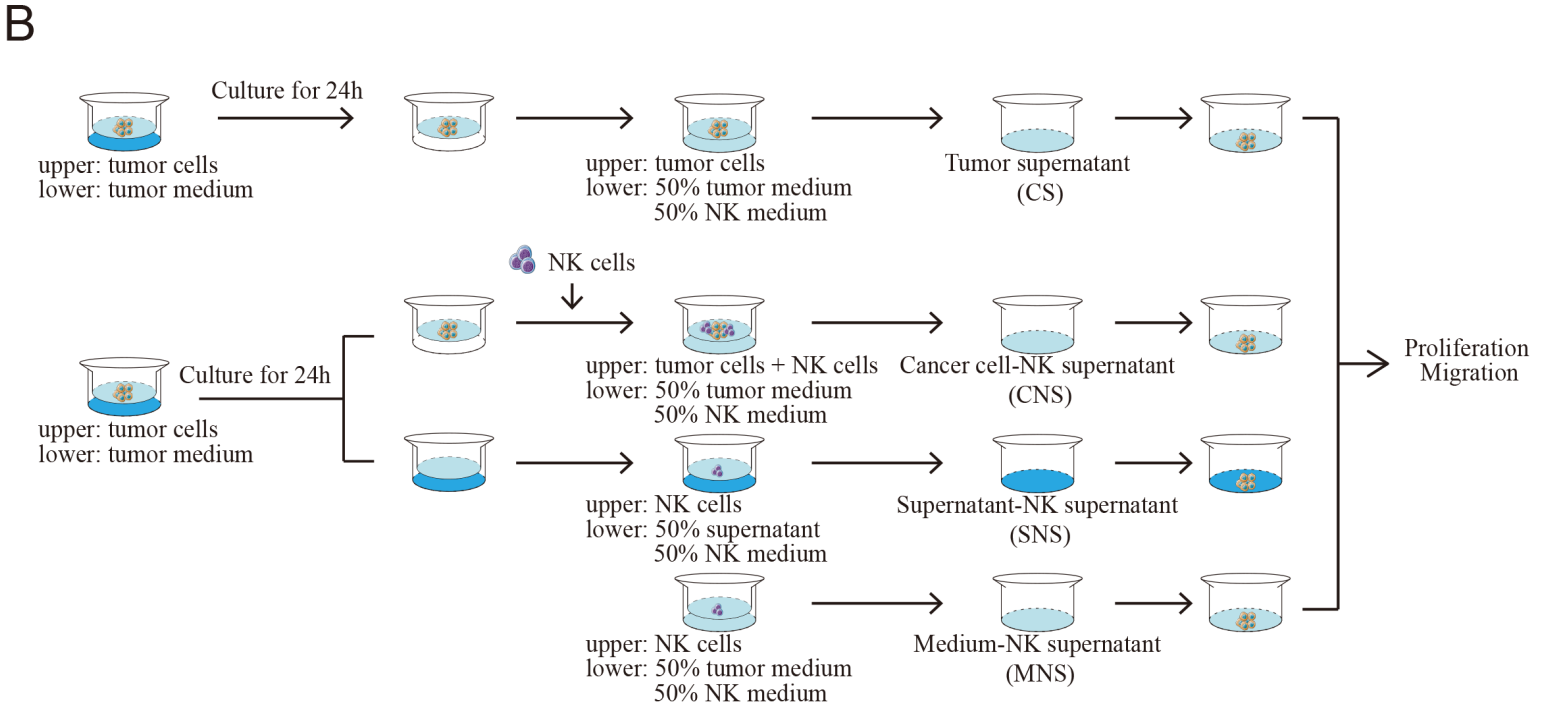
B
Culture for 24h
upper: tumor cells
lower: tumor medium
upper: tumor cells
lower: 50% tumor medium
50% NK medium
Tumor supernatant
(CS)
NK cells
Culture for 24h
upper: tumor cells
lower: tumor medium
upper: tumor cells + NK cells
lower: 50% tumor medium
50% NK medium
Cancer cell-NK supernatant
(CNS)
Proliferation
Migration
upper: NK cells
lower: 50% supernatant
50% NK medium
Supernatant-NK supernatant
(SNS)
upper: NK cells
lower: 50% tumor medium
50% NK medium
Medium-NK supernatant
(MNS)

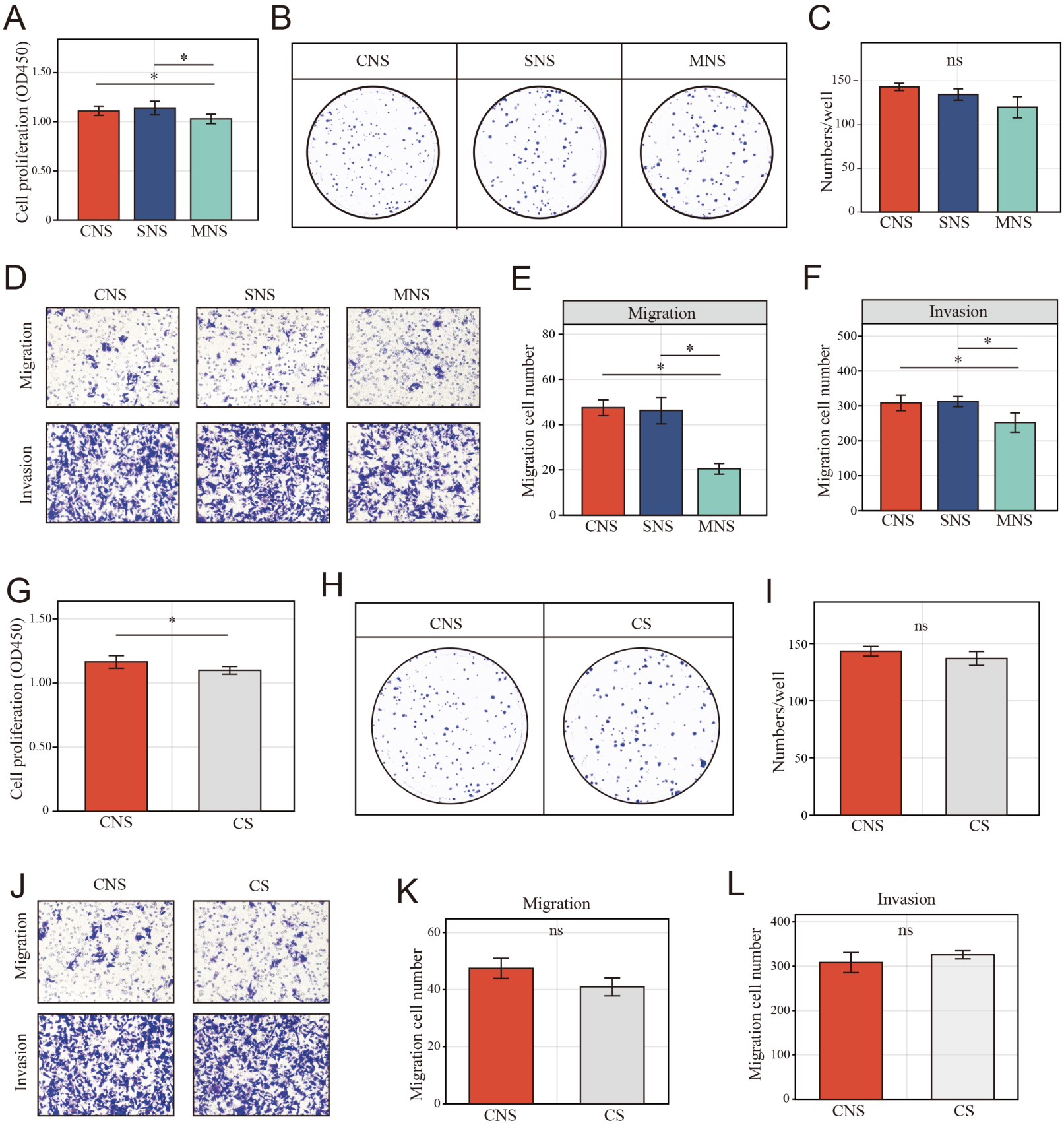
A
Cell proliferation (OD450)
1.50
1.00
0.50
0
*
*
CNS
SNS
MNS
B
CNS
SNS
MNS
C
ns
Numbers/well
150
100
50
0
CNS
SNS
MNS
D
CNS
SNS
MNS
Migration
Invasion
E
Migration
Migration cell number
80
60
40
20
0
*
*
CNS
SNS
MNS
F
Invasion
Migration cell number
500
400
300
200
100
0
*
*
CNS
SNS
MNS
G
Cell proliferation (OD450)
1.50
1.00
0.50
0
*
CNS
CS
H
CNS
CS
I
ns
Numbers/well
150
100
50
0
CNS
CS
J
CNS
CS
Migration
Invasion
K
Migration
ns
Migration cell number
60
40
20
0
CNS
CS
L
Invasion
ns
Migration cell number
400
300
200
100
0
CNS
CS

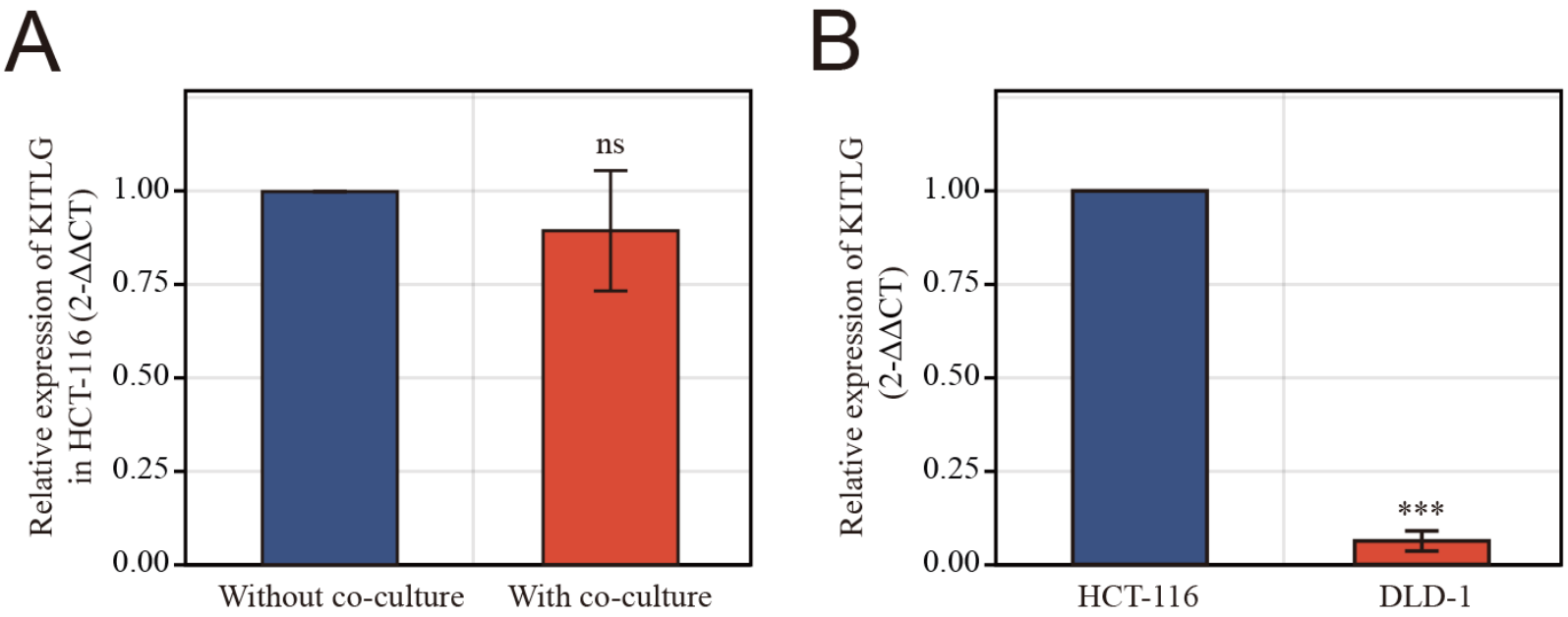
A
Relative expression of KITLG in HCT-116 (2-ΔΔCT)
1.00
0.75
0.50
0.25
0.00
ns
Without co-culture
With co-culture
B
Relative expression of KITLG (2-ΔΔCT)
1.00
0.75
0.50
0.25
0.00
***
HCT-116
DLD-1